UNIVERSITY OF TWENTE.

Faculty of Electrical Engineering,
Mathematics & Computer Science

A 2-layer 45° Slanted Phased Array Antenna with Baffles for 5G mmWave Applications Based on Gap Waveguide Technology

G.R. Meulman

M.Sc. Thesis
June 2020

Supervisors:
dr. A. Alayon Glazunov
A. Bagherimoghim

Radio systems Group
Faculty of Electrical Engineering,
Mathematics and Computer Science
University of Twente
P.O. Box 217
7500 AE Enschede
The Netherlands

Abstract

A phased array antenna is designed based on the gap waveguide technology which offers a fair trade-off between costs and manufacturing flexibility at the mmWave frequencies. Only two layers will be used to reduce manufacturing difficulty and costs. The final design consists of 8 parallel arrays of 8 slots each, and baffles are used to prevent grating lobes. The slots have been slanted 45 degrees for enabling easier polarization diversity. The antenna operates in the 26.5 - 29.5 GHz band, which is used for 5G applications. A average realized co-polar gain of 24.4 dBi is reached for a 0° scan angle, while keeping a total active reflection coefficient below -10 dB and a cross-polarization ratio of at least 25 dB.

Contents

1 Introduction

The demand for higher data rates and speed in cellular mobile networks is growing continuously. To fulfil this demand wider frequency bands in the order of GHz are needed. For the upcoming fifth generation technology standard for cellular networks (5G), this will be done by using frequency bands in the mmWave range. Also in other applications the use of mmWave frequencies is rising, for example in automotive anti-collision radar.

One of the frequency bands that will be used in 5G is (a subset of) the 26.5 - 29.5 GHz band. For example the USA and Canada have allocated the 27.5 - 28.35 GHz band, Japan has allocated the 27.5 - 28.28 GHz band, and South-Korea the entire 26.5-29.5 GHz band. A beamforming chip for this exact frequency band has already been made [1], but a low-loss and easy to manufacture antenna is still needed.

1.1 Existing designs

A well known method to design a high gain, high efficiency and low profile antenna is to use slotted waveguide array antennas. Their flat structure, low weight and the possibility to use electronic steering to rapidly change the main beam direction make these antennas attractive for many applications [2].

An importand issue with slotted waveguide antennas for mmWave frequencies is the complex manufacturing process, which will either result in very high costs, or possible leakage when gaps between different parts are not fully sealed. One proposed solution is to use a substrate integrated waveguide (SIW). Examples are a SIW fixed-beam array[3], and a SIW phased array[4]. These two antennas will be used for comparison in this thesis.

One of the drawbacks of a SIW antenna is the increased dielectric loss due to the presence of a substrate. A new way to solve the issue of leakage without using a substrate is the gap waveguide technology. Gap waveguides have emerged as a candidate for providing a fair trade-off between cost and manufacturing flexibility of electromagnetic components [5].

Two examples of gap waveguide antennas will be used for comparison in this thesis: a dual polarized gap waveguide antenna [6], and a phased array gap waveguide antenna [7]. An important difference between these two designs, and also between the two SIW designs, is the polarization of the slots. The fixed-beam SIW and the dual polarized gap waveguide antenna both have their slots slanted at a 45° angle. The slanted slots are an important design property that is wanted to increase polarization diversity in base stations as will be explained in chapter 2.1.5 [8].

1.2 Problem statement

For a 5G mmWave antenna, multiple design properties are wanted. It should be a phased array to be able to do beam steering and slanted slots are needed to increase polarization diversity. Furthermore it should also be not too difficult to manufacture without reducing the gain too much, for example by using 2-layer gap waveguide technology.

The existing designs given above all contain some of these properties, but an antenna design that contains all of these wanted properties doesn't exist yet.

1.3 Main contributions

This thesis presents two possible designs for a phased array antenna with slanted slots based on 2-layer gap waveguide technology for 5G applications in mmWaves. It is composed of 4 or 8 center fed subarrays, each containing 8 slots with a 45° slant.

2 Theoretical background

In this chapter the theoretical background will be given on antenna design. First, the main properties of an antenna in general will be discussed. Then the theory behind a phased array will be given, followed by an explanation on properties specifically important for phased arrays. Furthermore gap waveguide technology will be discussed, explaining how it works and what the advantages are.

2.1 Antenna properties

In this paragraph the main properties of an antenna will be discussed. These properties have to be taken into account while designing a new antenna as the results on these properties will form the basis of a comparison with other existing designs.

2.1.1 Antenna efficiency

Antennas are used to convert energy from the transmission line into radiated energy or vice-versa. Unfortunately, not all energy is perfectly converted from one to the other. For example a small part of the energy will be lost (converted to heat) due to dielectric losses in the antenna. The ratio between the input power and radiated power is called the antenna efficiency.

The antenna efficiency (e_0) is calculated as:

$$e_0 = e_r e_c e_d \tag{1}$$

In this equation e_r is the reflection efficiency, expressing the losses due to mismatch between the transmission line and antenna. e_c is the conductive efficiency, containing the losses due to finite conductivity of the metal that forms the antenna. e_d is the dielectric efficiency, taking into account the losses due to conductivity of a dielectric material in or near an antenna. In general a total antenna efficiency above -1 dB is considered sufficient.

2.1.2 Directivity, gain and realized gain

One of the most important figure-of-merits for an antenna is the directivity. The definition of directivity is given by the International Electrotechnical Commission (IEC) as: "The ratio of the radiation intensity in a given direction from the antenna to the radiation intensity averaged over all directions". This means directivity is not just a single value, but a complete pattern with a value for every direction. Directivity is usually expressed in dBi, which is the radiation intensity compared to a hypothetical isotropic antenna. An isotropic antenna is the idea of an antenna that has an equal radiation intensity in all directions.

A closely related figure-of-merit to directivity is gain. Next to the directional properties the gain also takes the radiation efficiency of the antenna into account. This means from the total antenna efficiency expressed in equation 1 only the conductive efficiency (e_c) and dielectric efficiency (e_d) are taken into account. This radiation efficiency is multiplied with the directivity to get the gain.

When the total antenna efficiency including the reflection efficiency (e_r) is taken into account, the term realized gain is used. In this thesis realized gain will be mainly used, as this shows best how well the antenna as a whole performs in real situations.

2.1.3 Reflection coefficient

The reflection efficiency is calculated with $e_r = (1 - |\Gamma|^2)$, where Γ is the reflection coefficient. The reflection coefficient is a parameter that describes how much of a wave is reflected by an impedance discontinuity in a transmission medium, in this case between the transmission line and antenna. The reflected energy is not accepted by the antenna, and therefore lowers the efficiency of the antenna. The reflection coefficient is equal to the ratio of the amplitude of the reflected wave to the incident wave, expressed in dB. In this thesis the scattering parameter S_{11} will be used instead of Γ, as they are equal. A maximum reflection coefficient of -10 dB is required for the antenna that will be designed, comparable to other existing designs.

2.1.4 Main beam and side lobes

As discussed in paragraph 2.1.2 the gain or realized gain of an antenna is not just a single value but a pattern with different values for every direction. When only a single value is given, the gain in the main lobe is meant. The main lobe, also called main beam, of an antenna is the radiation lobe in the direction of the highest gain.

A radiation lobe is a part of the radiation pattern with a relatively high intensity, bounded by a region with relatively low intensity. A common way to quantify the size of such a lobe in a plane is the half power beamwidth (HPBW), which is the angle between the -3dB points on both sides of the maximum.

Next to the main lobe there are also side lobes. Side lobes are radiation lobes in any other direction than the main lobe and are usually unwanted. To make sure these side lobes do not have too much influence on the performance, the difference between the main lobe and side lobes should be at least 10 dB. This difference between main lobe and the highest side lobe is called the side lobe level.

2.1.5 Polarization

The polarization of an electromagnetic wave is the plane in which the electric field oscillates, as visualised in figure 1. The polarization can also be cylindrical or elliptic, but this will not be explained here as linear polarization will be used only in this thesis.

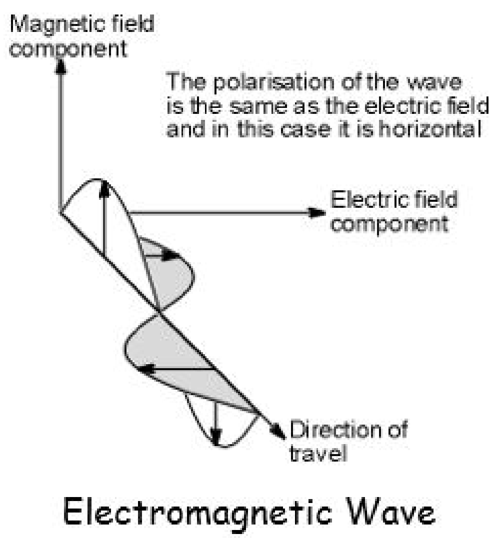

Figure 1: Visualization of polarization of EM-wave

For a polarized antenna, a wanted polarization is defined. This can be horizontal, vertical or slanted at an angle. The electric field vector of an outgoing wave is decomposed in a wanted part (co-polarization) and the unwanted perpendicular part (cross-polarization). An example is given in figure 2. Here the wanted polarization is at a 45° slant. The electric field vector however is not exactly in this same direction, so it is

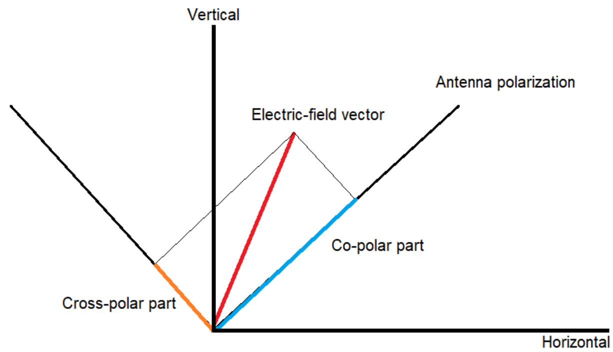

Figure 2: Decomposition of co- and cross-polar parts of electric field

decomposed in a co-polar and cross-polar part. To calculate the co-polar gain, only the intensity of the co-polar part of the electric field vector is taken into account. The ratio between the gain in the co-polarization and cross-polarization is called the cross-polarization ratio (XPR), and a minimum XPR of 20 dB is preferred.

To increase the capacity and the reliability of a wireless system and combat multi-path fading, orthogonally polarized antennas can be used [9]. An antenna system that uses two orthogonal polarizations for this purpose is called dual-polarized. For base stations in telecommunication it is very important to have this polarization diversity [8].

In a dual polarized antenna system it is important that the performance of both polarizations is as equal as possible [10]. When using a horizontal/vertical polarization this will be very difficult to achieve as the design of both antennas and waveguide structure will be very different [11]. When using a 45° slant for the slots however, the exact same antenna with only the radiation layer mirrored can be used for the other polarization. This will result in practically the same performance, with only the radiation pattern mirrored.

A visualization of the direction of a slanted polarization and the E-plane, H-plane and D-plane is given in figure 3. Here a top view of a single array element with 45° slanted slots is shown.

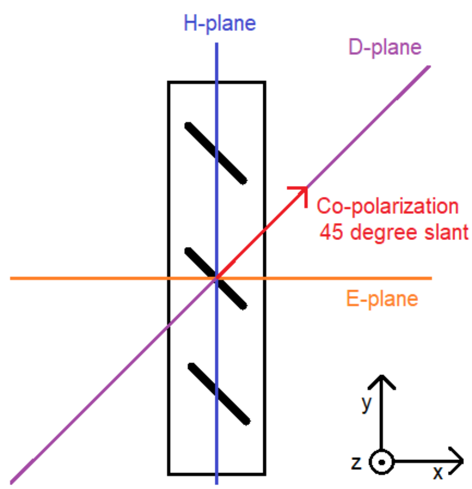

Figure 3: Visualization of E-, H-, D-plane and slanted co-polarization direction

Using non-slanted slots and instead rotating the entire antenna is not an option as the E-plane, in which beam steering can be done, will also rotate in that case.

2.1.6 Bandwidth

The bandwidth of an antenna is defined as the frequency range within which the performance of the antenna conforms to a specified standard. The bandwidth of an antenna is expressed as a percentage of the frequency difference over the the center frequency. The frequency range that will be used in this research is 26.5 to 29.5 GHz, which means a bandwidth of 10.7%.

2.2 Phased array principles

The antenna that will be designed in this research is a phased array. A phased array is an array of antennas which creates a beam of radio waves that can be electronically steered to different directions. The steering, called beamforming, is done without moving the antennas, instead the phase of every antenna in the array is changed.

A phased array is based on the path length difference of an incident signal to different antennas within the array. A schematic explanation is shown in figure 4. When an incident signal has an angle from zenith (θ) other than 0°, the difference in path length to two antennas is $d \cdot sin(\theta)$, where d is the distance between the two antennas. Because the signals should be in phase before they are added together, this difference in path length needs to be compensated for. This is done by applying a phase delay to the signal of the first antenna corresponding to the ratio between the difference in path length and the wavelength.

The addition of a certain phase delay only works for the corresponding angle, as different delays are needed for different angles. This means that for all other angles the signals at antenna 1 and 2 will not be in phase, and no constructive interference takes place. Therefore the direction of tranceiving of an antenna can be aimed at different directions by changing the phase delay between the antennas in the array.

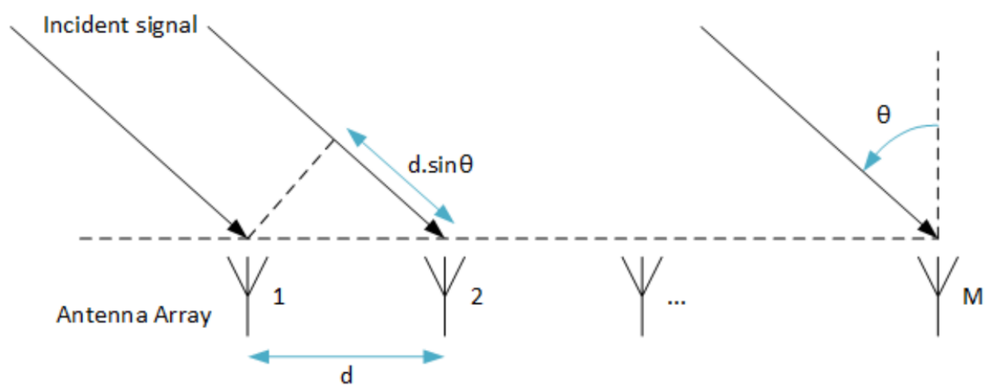

Figure 4: Path length difference in a phased array [12]

2.3 Array antenna properties

In this paragraph the main properties of an array antenna will be discussed. Next to the general antenna properties discussed in the first paragraph, there are also antenna properties specific for antenna arrays. These properties will also be taken into account when comparing the new designs with existing designs.

2.3.1 Mutual coupling

Mutual coupling is the electromagnetic interaction between the antenna elements in an array. Mutual coupling is typically undesirable because energy that should be radiated away is absorbed by a nearby antenna instead. Hence, mutual coupling reduces the antenna efficiency and performance of antennas. Another reason why mutual coupling is unwanted is the change in radiation pattern. The energy absorbed by a nearby antenna is partially re-radiated, resulting in constructive and destructive interference that alters the radiation pattern.

In this report the mutual coupling is described in S-parameters. $S_{1,2}$ for example is the mutual coupling between element one and two. For the antenna that will designed a mutual coupling below -20 dB is preferred.

2.3.2 (Total) active reflection coefficient

The active reflection coefficient (ARC) is the reflection coefficient for a single antenna element in an array antenna in the presence of mutual coupling. The ARC does not only depend on frequency, but also on the excitation of the other elements. When using a phased array the phase difference between the excitations differ for every scan angle, and therefore the ARC is different for every scan angle too.

The Total active reflection coefficient (TARC) is the reflection coefficient of all elements of the array combined. The TARC is the square root of the sum of all reflected power, divided by the square root of the sum of all incident power of the antenna array. It is still dependent on the excitation of the elements, and therefore also dependent on the scan angle.

2.3.3 Grating lobes

Grating lobes are side lobes that occur due to the constructive interference of the radiation pattern of multiple antenna elements in an array, other than the main beam. Grating lobes occur when the distance between the radiating slots is larger than λ, or when the distance is between 0.5 λ and 1 λ if beamforming is used. The phase difference between the received signal at elements for certain directions other than the wanted direction can be exactly one ore multiple wavelengths. Grating lobes have usually the same size as the main beam and are just like other side lobes unwanted.

For phased arrays, a maximum angle from zenith can be defined in which grating lobes will not occur. This maximum angle depends on the distance between the array elements, and can be calculated with:

$$d_{max} = \frac{\lambda}{1 + sin(\theta)} \tag{2}$$

In this equation θ is the needed maximum angle and d_{max} is the corresponding maximum distance between the radiating array elements. For this antenna design a 45 degree look angle is desired. This means that a maximum distance between the array elements of 0.58 λ is allowed.

When a transversal waveguide is used the slots can only be placed every λ_w instead of every 0.5 λ_w, where λ_w is the wavelength in the waveguide. As λ_w is usually around 1.4 times larger than the wavelength in free space (λ), this means the distance between the slots will be a lot larger than 1 λ which will therefore result in grating lobes.

2.3.4 Baffles as a spatial filter for grating lobes

To reduce grating lobes, baffles can be used [13]. Baffles are walls between the radiating slots that will reduce grating lobes by directing the waves to the wanted direction increasing the gain in the main beam.

In the antenna near-field region close to the source a reactive field exists. When sources are placed close to each other these fields will cancel out, but when the distance is too large, the reactive fields will start to radiate. By radiating into a parallel plate region, between the baffles, the wavelength can be controlled in that region by the spacing between the parallel plates (a in figure 5). Only the main beam and no grating lobes will radiate when $a > a_1 > \lambda/2$.

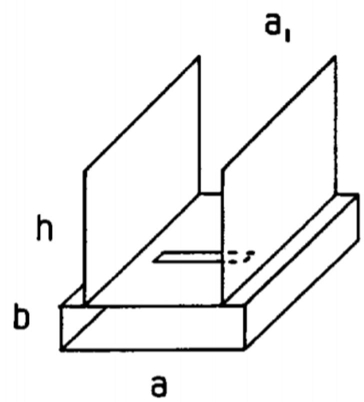

Figure 5: Transverse slot in rectangular waveguide with parallel plates (baffles) [13]

2.4 Gap waveguide technology

An importand issue with slotted waveguide antennas for mmWave frequencies is the complex manufacturing process, which will either result in very high costs, or possible leakage when gaps between different parts are not fully sealed.

A new way to solve the issue of leakage and a complex manufacturing process is the gap waveguide technology. Gap waveguide technology has emerged as a candidate for providing a fair trade-off between cost and manufacturing flexibility of electromagnetic components [5].

The fundamental operating principle of gap waveguide technology is based on the cutoff of propagating waves in a PEC/PMC parallel-plate configuration. When the gap between the two plates is smaller than $\lambda/4$, no wave can propagate between the plates due to the existing PEC/PMC boundary conditions [14]. This is also shown in figure 6.

The PMC condition is artificially realized by emulating the high impedance boundary condition of a PMC surface. In gap waveguides, this is realized in the form of periodic metal pins with air gaps in between. When the air gap is smaller than quarter wavelength there is a cutoff of all propagating modes within the gap due to the high surface impedance. By keeping a large open space the size of the waveguide, a PEC-like plate is realized which will support the TEM wave as shown in figure 6 (b).

The pins can be easily manufactured on the bottom plate. When the top plate is added to form the waveguide, the sealing between the pins and the top plate is not critical anymore, opposite to conventional metal tube waveguides.

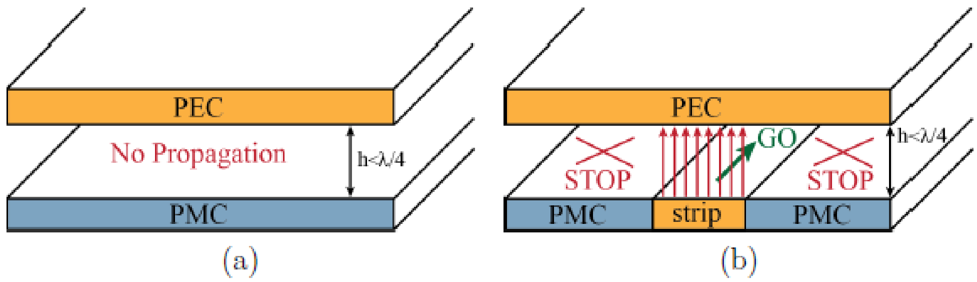

Figure 6: Basic operating principle of gap waveguide: (a) PEC-PMC Parallel-plate EM-wave cutoff. (b) TEM local wave propagation [14]

2.4.1 Groove gap waveguide

When a vertical (transversal) waveguide is used, it is also possible to use gap waveguide technology [15]. Some small adjustments are needed to make it work as the height of the pins would exceed the $\lambda/4$ limit, which would allow waves to propagate in the small air gaps between the pins. Furthermore the manufacturing of such high but small pins would not be feasible either.

Instead, a groove gap waveguide design is used. A comparison of a "standard" horizontal gap waveguide and a groove gap waveguide is shown in figure 7. In a groove gap waveguide only the upper part of the sides of the waveguide is replaced with pins, not exceeding the $\lambda/4$ limit. The bottom part consists of solid walls without air gaps in between.

(a) Horizontal waveguide: E_x

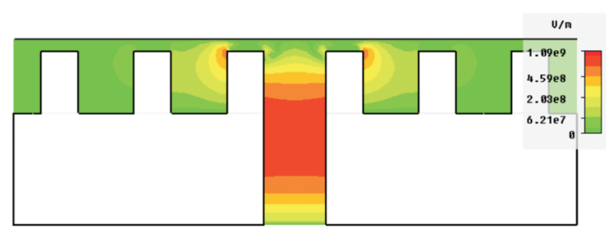

(c) Vertical waveguide: E_x

(b) Horizontal waveguide: E_y

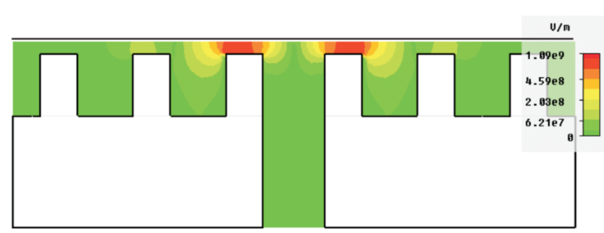

(d) Vertical waveguide: E_y

Figure 7: 2D-color plots of the TE-field for frequencies within the single mode band [15]

3 Design methodology

In this chapter the design procedure will be discussed. Simulation conditions and assumptions will be given, and design choices will be explained.

3.1 Design procedure

The goal of this research is to design a phased array antenna, but to reach this goal a start is made at a much smaller scale. First with pins only, followed by a waveguide, a single antenna element and finally the complete array.

To determine the dimensions of the pins of the gap waveguide, the dispersion diagram of a periodic unit cell will be used as is explained by P.-S. Kildal [16]. This periodic unit cell is shown on the left in figure 8, and contains one pin and both x and y boundaries are set to periodic. With the eigen-mode solver from CST MWS, the dispersion diagram can be created. In the dispersion diagram it can be seen whether the stop-band covers the entire frequency range of interest. The simulated pins function as a proper isolating wall within this stop-band.

Next, a model of the waveguide as shown on the right in figure 8 is simulated. This model is periodic in the y-axis but finite in the x-axis with magnetic boundaries. Again, the eigen-mode solver from CST is used to obtain the dispersion diagram. Because a wave has to propagate through the waveguide, there should not be a stop-band in the frequency range of interest, but instead only one mode should be present to make it single mode.

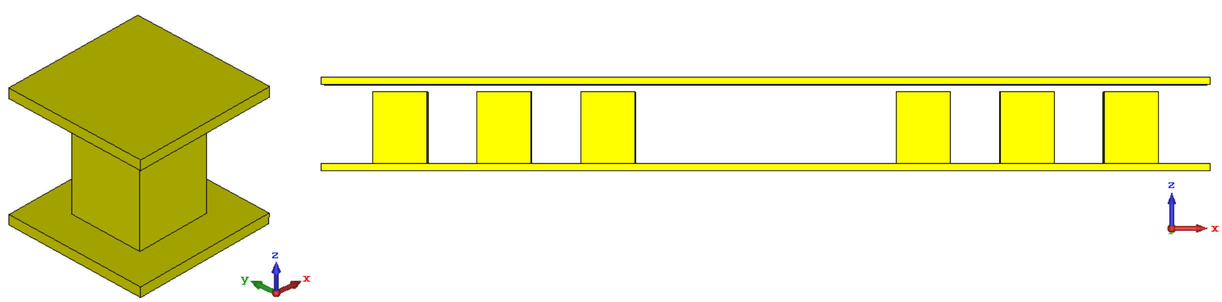

Figure 8: The single periodic pin model (left) and the periodic waveguide model (right)

When the right dimensions for the waveguide have been chosen, a single antenna element can be designed and simulated. In this thesis, two different designs will be elaborated on: a horizontal gap waveguide antenna (design 1) and a transverse or vertical groove gap waveguide antenna (design 2). The used dimensions for every element are based on the previous designs that are also used for comparison in this thesis. To optimize the design, these dimensions have been varied and the values with the best results based on the antenna parameters mentioned in chapter 2 have been chosen. In this report only the final dimensions will be given.

The final design for the single element of the horizontal and vertical gap waveguide antenna are shown in the first part of chapter 4.2 and 4.3 respectively. The antenna elements are simulated in three different situations: a single element in free space, a single element embedded at the edge of an array and a single element embedded in the middle of an array. This way the influence of other elements in an array can be verified.

Furthermore a four-element phased array as a whole is simulated. For the phased array, four single elements are added next to each other, all with the same polarization. Ports will be excited simultaneously, and with adding a phase shift the resulting beam is steered to different directions. To reduce simulation resources, the array consists of only four elements instead of eight like the arrays that are used for comparison. When the results of the four-element array are found sufficient, a eight-element array is simulated to be able to make a better comparison.

3.2 Simulation conditions and assumptions

The material used for the antenna elements in this thesis is the standard lossy aluminium from CST MWS ($\mu = 1, \sigma = 3.56e7$). This material is also used in simulations of other designs like the two gap waveguide antennas and the SIW phased array that are used for comparison in this thesis.

Different boundary conditions are used in the different simulation setups. For the periodic unit cell pin simulations the x- and y-boundaries are set to periodic, and the z-boundaries to electric conducting wall. For the eigen-mode solver simulations on the waveguide the x-boundaries are set to magnetic conducting, similar to previous research [16]. In all other simulations the boudaries are set to "open (add space)", except for the negative z-boundary behind the antenna which is set to electric conducting wall.

3.3 Design choices

Two different antenna models are designed and tested in this thesis. The first design is a horizontal gap waveguide and the second design is a vertical or transversal groove gap waveguide. Next to these standard waveguide layouts several design choices have been made to improve the performance of the antenna designs. A picture of design 1 showing these design choices is given in figure 9.

One of the choices that had to be made was the number of slots, and therefore also the length of the antenna

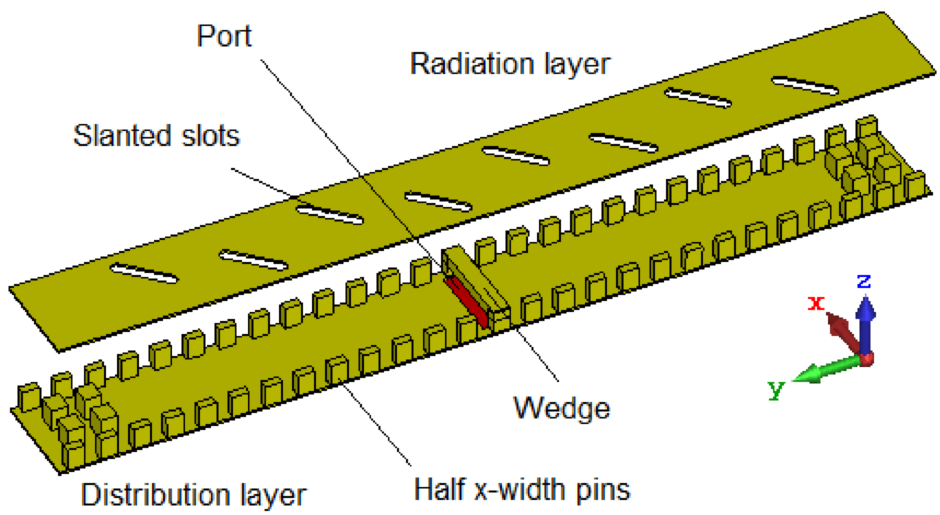

Figure 9: Model of design 1 with implemented design features

element. The amount of slots that has been chosen is eighth, as this gives a good trade-off between gain and bandwidth. More slots and therefore a longer waveguide result in a larger difference in phase between different frequencies and thus reduces the bandwith. Increasing the amount of slots to 10 would decrease the bandwith such that it was not possible to get a realized gain of at least 12 dB over the entire frequency range of interest.

Compared to previous gap waveguide designs with slanted slots, the number of layers has been reduced from three to two layers to increase manufacturability and therefore decrease costs.

The antennas are center fed, as this increases the symmetry of the field pattern. Also the total length of the waveguide can be twice as long without changing the length between the port and the reflecting end of the waveguide. The two other gap waveguide antennas that are used for comparison are center-fed too.

In the model it can be seen that a wedge is added in the centre opposite to the port connection. This is common in waveguide T-junctions and has been done to reduce the reflection coefficient [17]. In the model of design 2, shown in figure 10, it can be seen that this wedge is also made with gap waveguide technology, for similar reasons as it is used at the sides.

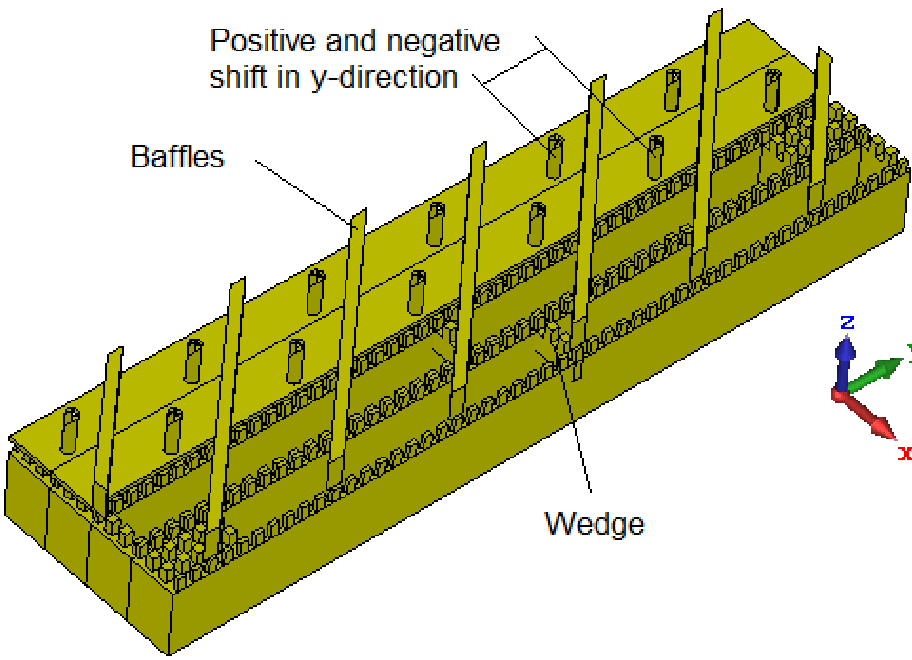

Figure 10: Model of design 2 with implemented design features (Half of the radiation layer is hidden)

The amount of pins between adjacent waveguides has been set to one, to keep the distance between the slots of different elements as small as possible. For the single element this means that only half of the pin is visible at each side, which will form a whole pin together with the half pin from the next element.

To increase the isolation between the different elements of the array, a shift of alternately $+0.25\lambda_w$ or $-0.25\lambda_w$ is added to the elements in design 2. From simulation it has been found that this distance shift of $0.5\ \lambda_w$ along the waveguide is optimal, which is in accordance with other related research [3].

Another design choice is the use of baffles in design 2. Due to the larger distance between the slots in a single element compared to design 1, grating lobes occurred as explained in chapter 2.3.3. To show the advantage of the baffles a comparison between an array with and without baffles is shown in figure 11. This shows the significant reduction of grating lobes while increasing the gain in the main beam.

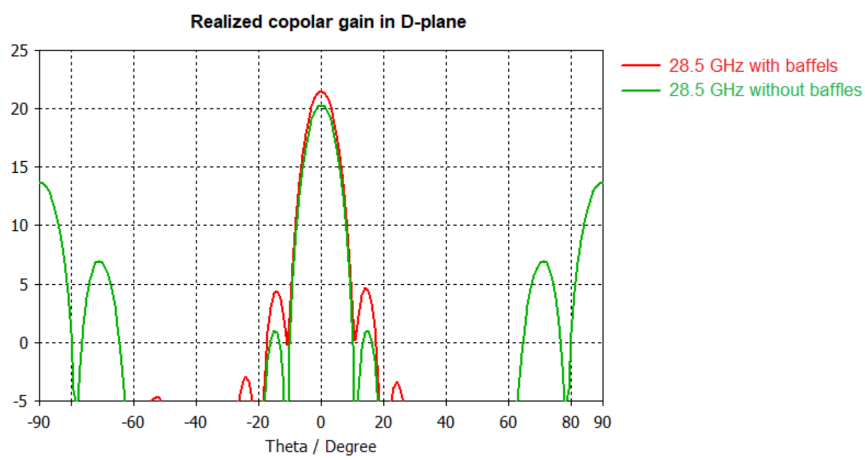

Figure 11: Gain pattern in D-plane with and without baffles

4 Results

4.1 Pin and waveguide design

The periodic unit cell and waveguide as shown in figure 8 are simulated with the eigen-mode solver from CST MWS software to obtain the dispersion diagrams. By simulation and optimization the following parameters have been chosen: $Pin_h = 2.2$, $Pin_w = 1.5$, $Pin_t = 1.4$ and $waveguide_w = 7.3$. These values and a description can also be found in table 1. The dispersion diagram of the periodic unit cell is shown on the left in figure 12 and the waveguide on the right.

From the dispersion diagrams in figure 12 it can be seen that the stopband of the pins goes from 18.2 GHz to 66.0 GHz and therefore covers the entire frequency band of interest. This means a row of pins with the chosen parameters are suitable as an isolating wall. From the dispersion diagram on the right it can be seen that the waveguide is single mode from 21.9 GHz to 54.8 GHz. This also covers the entire frequency band of interest, and therefore it can be concluded that a proper waveguide can be made with the chosen parameters.

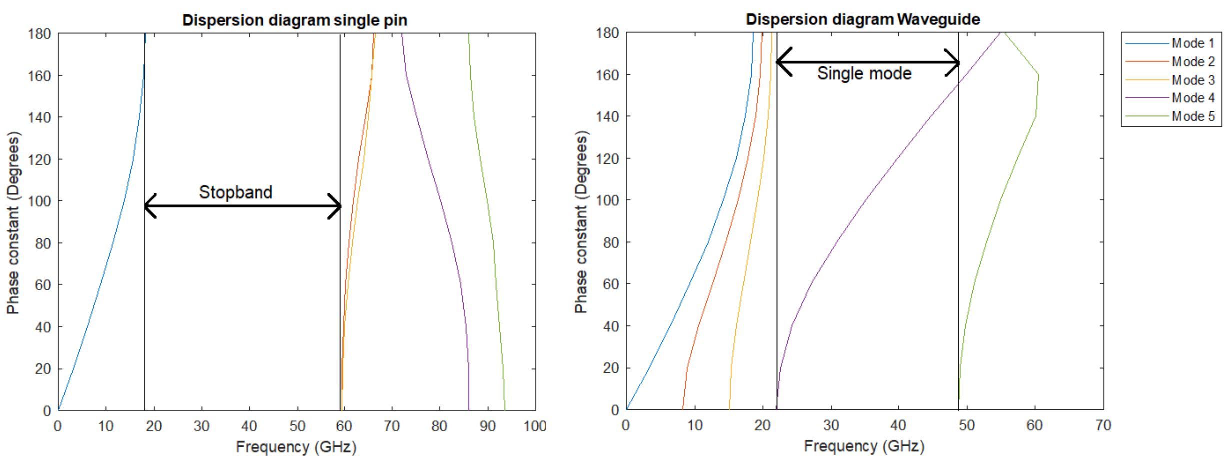

Figure 12: Dispersion diagram of a single periodic pin (left) and waveguide (right) of figure 8

Parameter	Size (mm)	Description
Pin_h	2.2	Height of the pins
Pin_w	1.5	Width of the pins
Pin_t	1.4	Space between pins
$Waveguide_w$	7.3	Width of the waveguide (between the pins)
$Waveguide_h$	2.2	Height of the waveguide (Pin_h)
$Waveguide_l$	66	Length of the waveguide (between the pins)
$Slot_w$	1.0	Width of the slots
$Slot_l$	5.7	Length of the slots
$Blend_r$	0.5	Blend radius of slot corners
$Slotdisty$	7.4	Spacing between the slots y-axis
$Slotdistx$	2.4	Displacement in +x or -x for every other slot
$Port_l$	7.3	Length of the port in bottom plate
$Port_w$	2.3	Width of the port in bottom plate
$Wedge_w$	1.5	Width of the wedge
$Wedge_h$	1.0	Height of the wedge (down from top plate)

Table 1: Parameter table Design 1

4.2 Design 1

In this chapter the results on design 1 will be given and commented on. First the designed model is given for both single element and an array. Then the results are given for a single element in free space, on the edge and in the center of an array, respectively. In the last part the results on the phased array as a whole are given.

4.2.1 Design models

The CST model of the single element can be found in figure 13. The gap between the distribution layer and radiation layer in the top picture has been overdrawn for visual purposes. The exact parameters can be found in table 1.

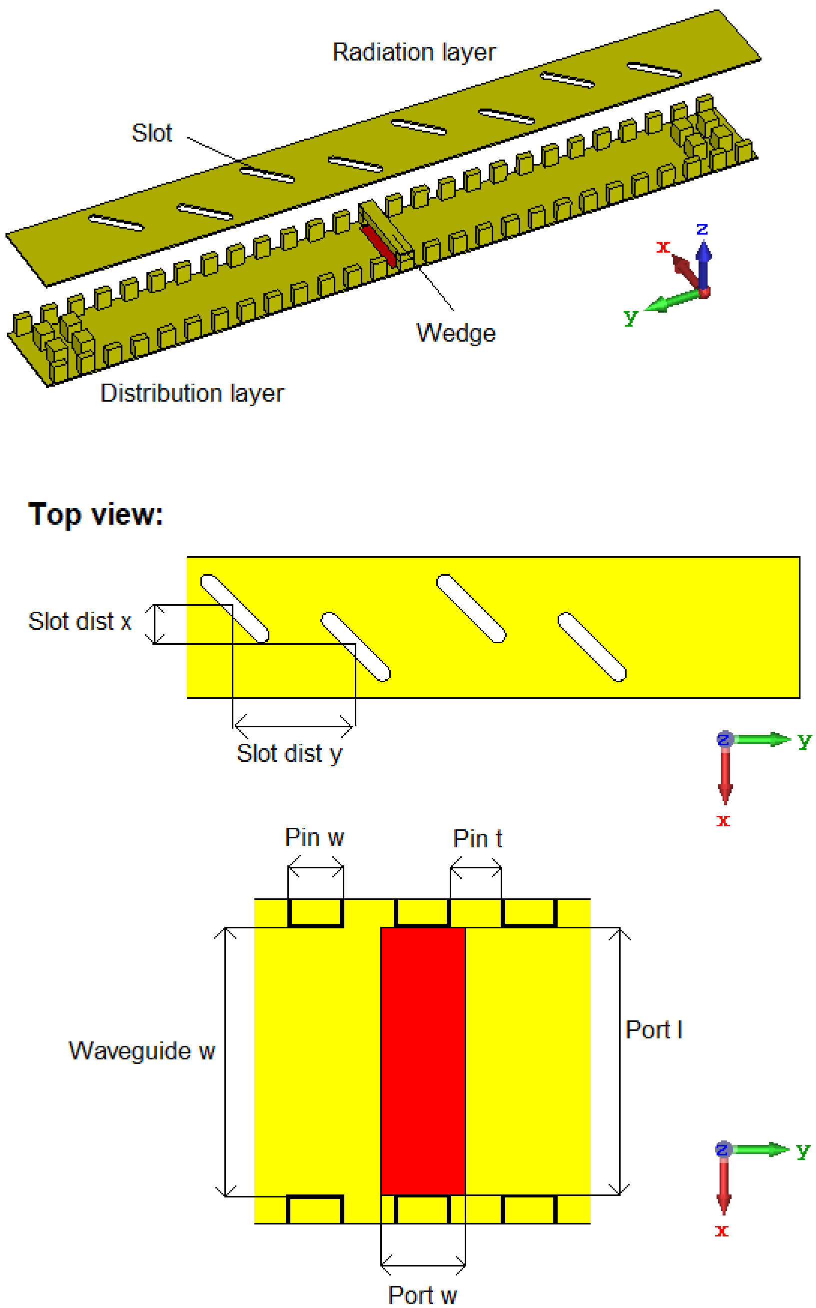

Figure 13: CST model of a single element of design 1

The CST model of the phased array of design 1 is shown in figure 14. The only difference is the addition of three extra elements. All design parameters from table 1 are still valid.

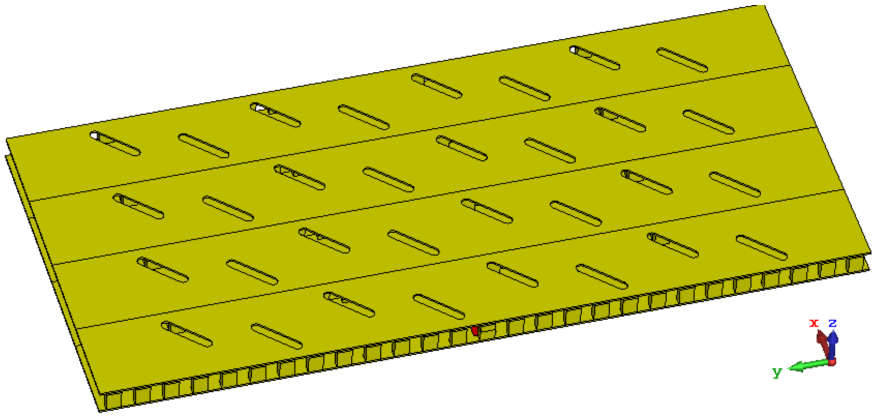

Figure 14: CST model of 4-element phased array of design 1

4.2.2 Single element results

First, the results on a single element in free space are given. The co-polar and cross-polar gain in the E-, H- and D-plane can be found in figure 15 and 16 respectively. From the results it can be seen that the gain pattern is especially wide in the E-plane and not in the H-plane. This was expected, and is also needed later on for beamforming. The cross-polarization gain is very low, which results in a cross-polarization level of at least 25 dB in the center.

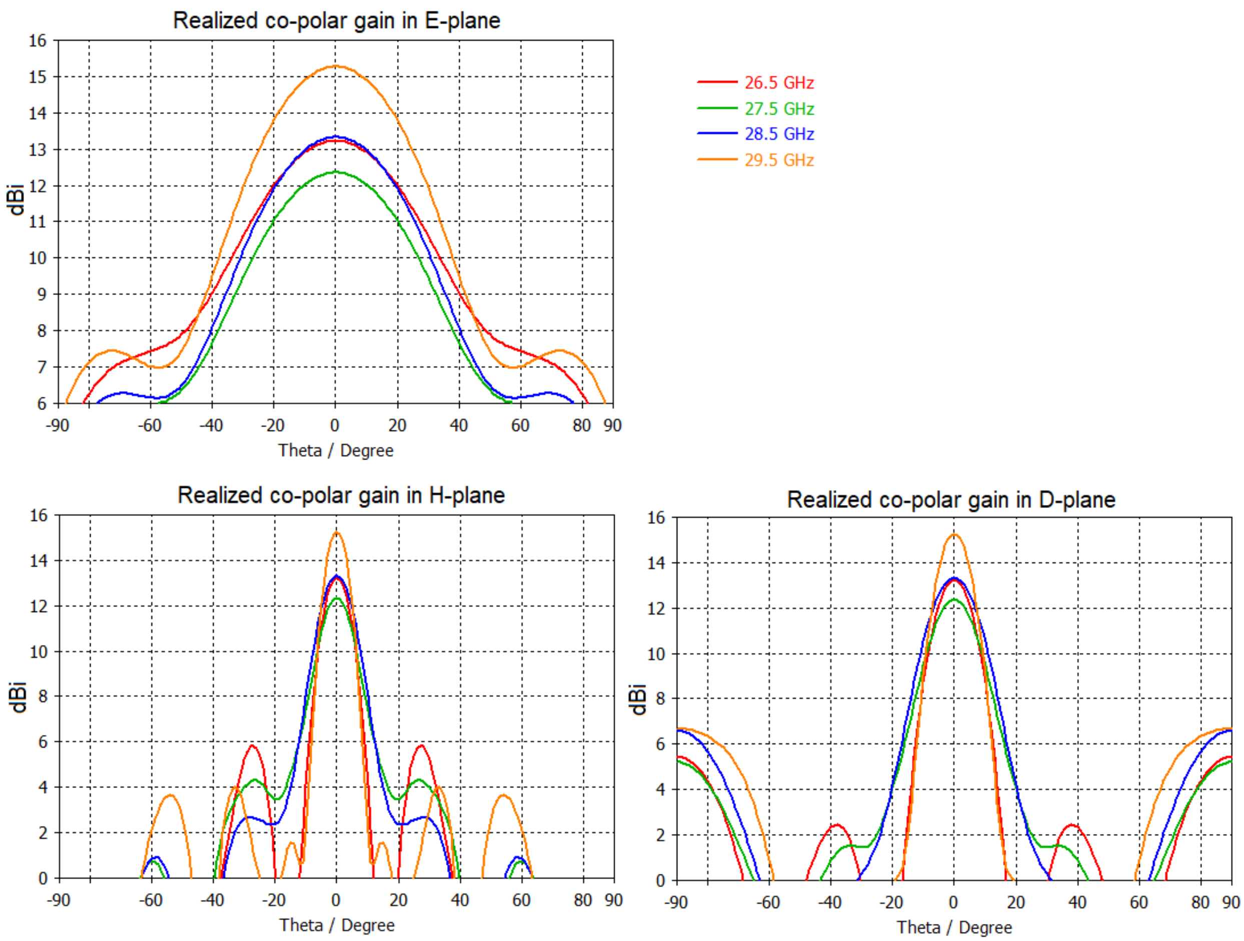

Figure 15: Co-polar gain of single element in free space of design 1

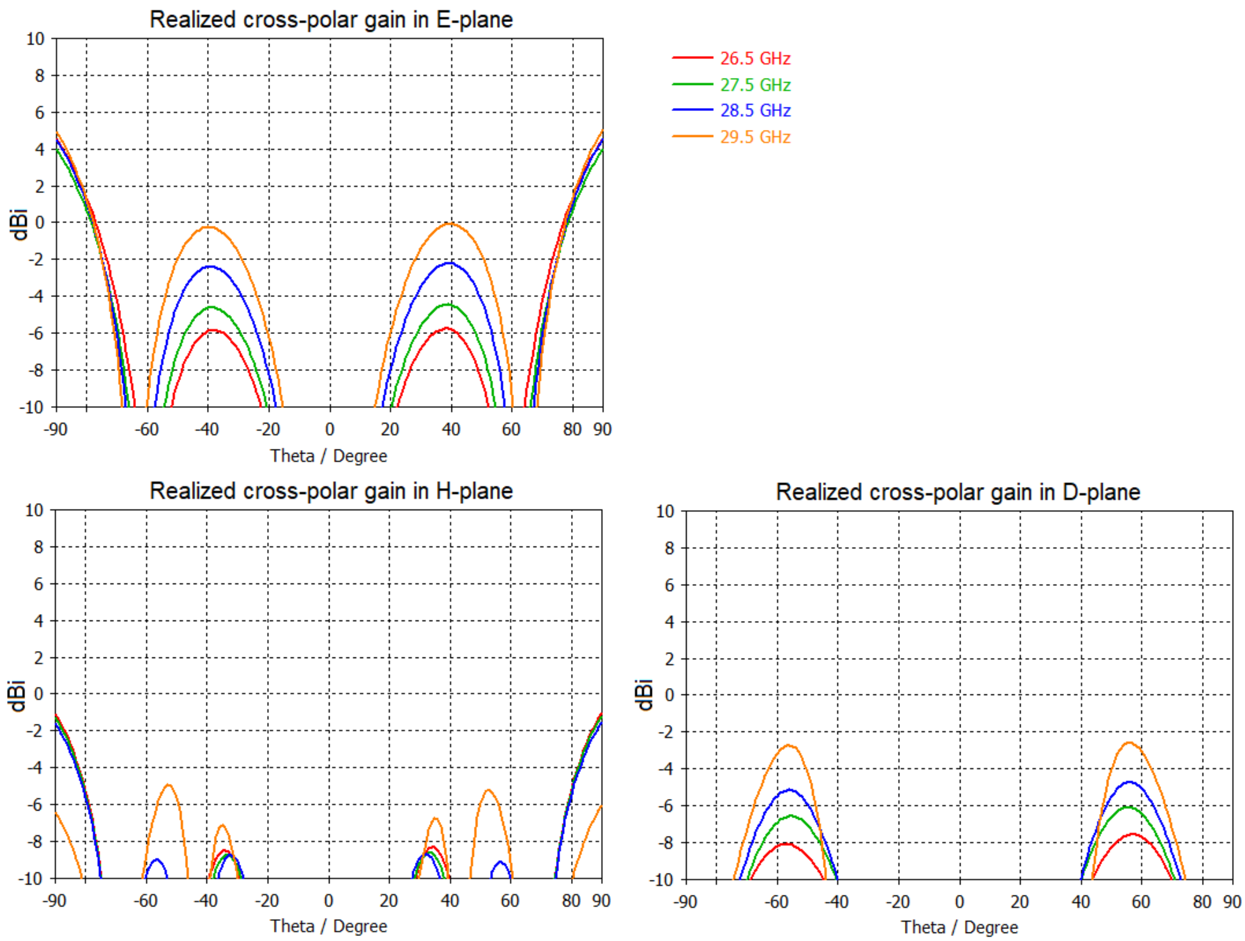

Figure 16: Cross-polar gain of single element in free space of design 1

In figure 17 the reflection coefficient of the single element is shown. Between 26.5 and 29.5 GHz the reflection coefficient is below -12 dB, which satisfies the maximum of -10 dB. In figure 18, the maximum realized gain as a function of frequency is shown. It is already visible that the gain is not very stable over frequency with a difference of almost 3 dB between 28.0 and 29.5 GHz. Although no requirement for this difference was specified, it is definitely a drawback.

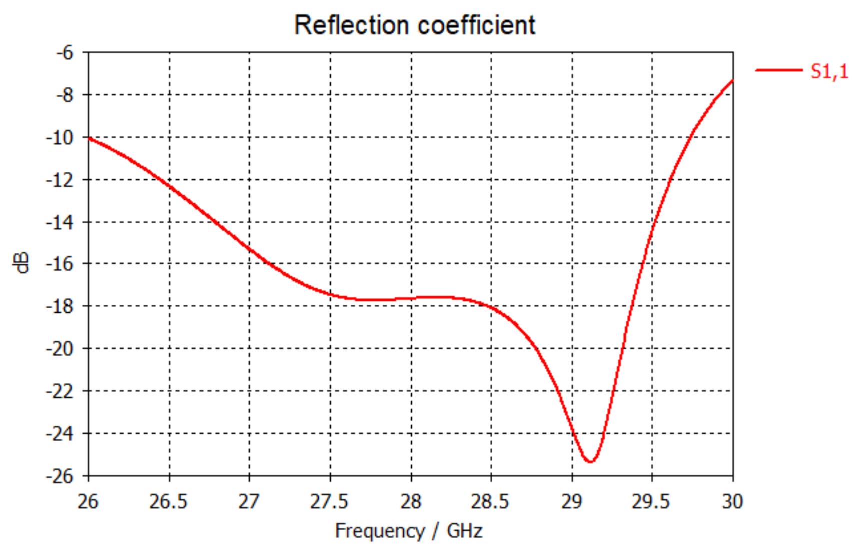

Figure 17: Reflection coefficient of single element in free space of design 1

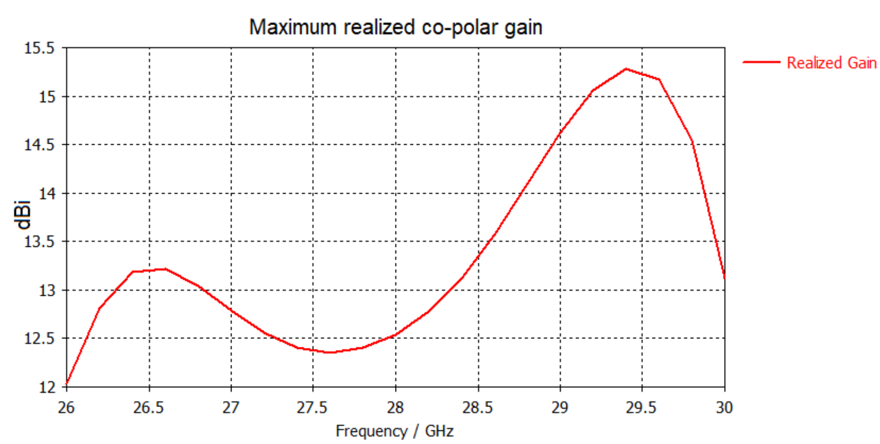

Figure 18: Maximum realized co-polar gain of single element in free space of design 1

4.2.3 Embedded element results

Next, the results on a single element on the side of a four-element array is given. The co-polar and cross-polar gain in the E-, H- and D-plane can be found in figure 19 and 20 respectively. Also the co- and cross-polar gain for a center element (element 2) are given, these can be found in figure 21 and 22.

Comparing the results of the edge and center element it can be seen that the main beam of the edge element is slightly shifted from the center in the E-plane, pointing at an angle of approximately -10°. Beyond that the differences are not very large. The values for maximum gain are comparable, and the cross-polarization gain is very low for both.

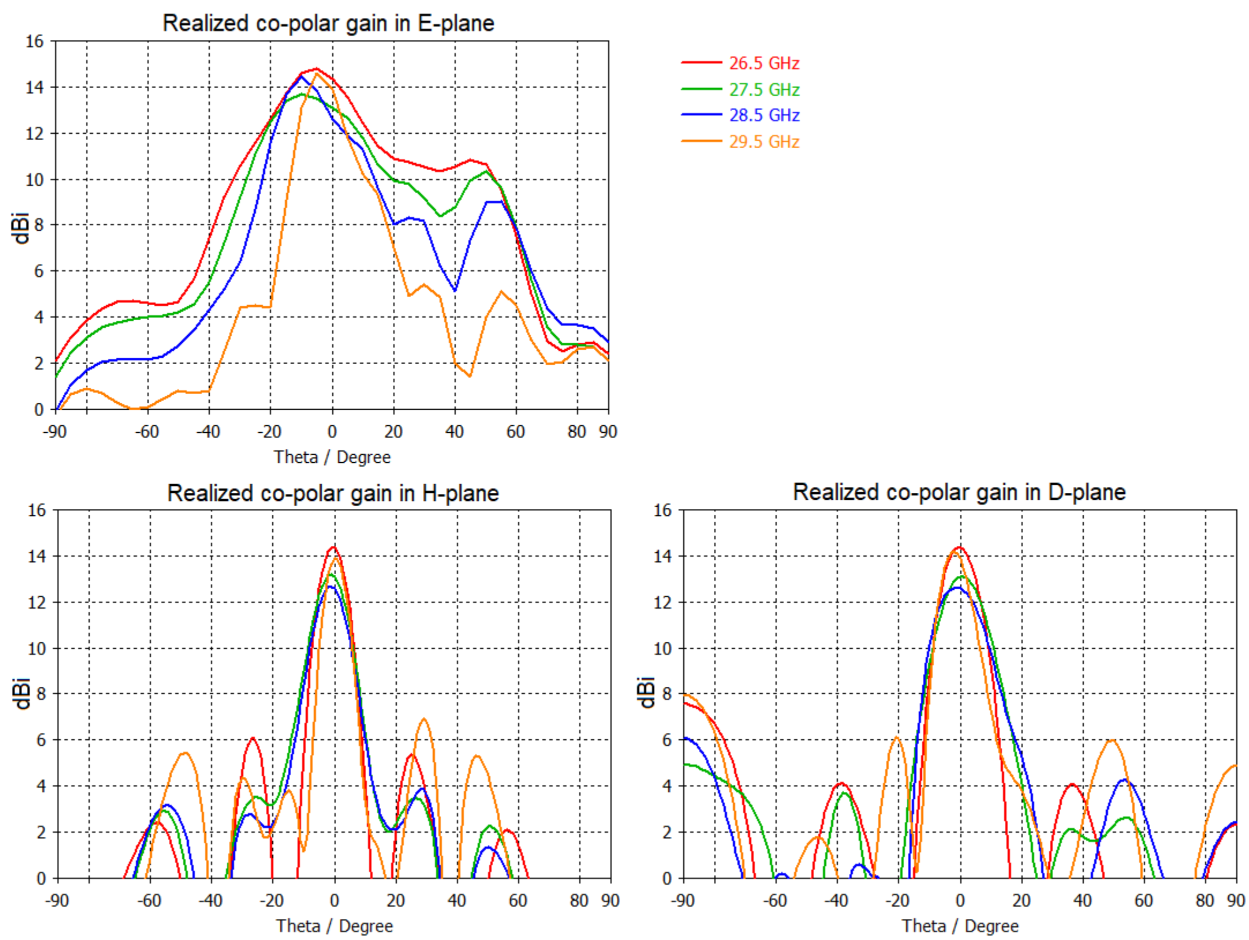

Figure 19: Co-polar gain of design 1 element embedded on the side of an array

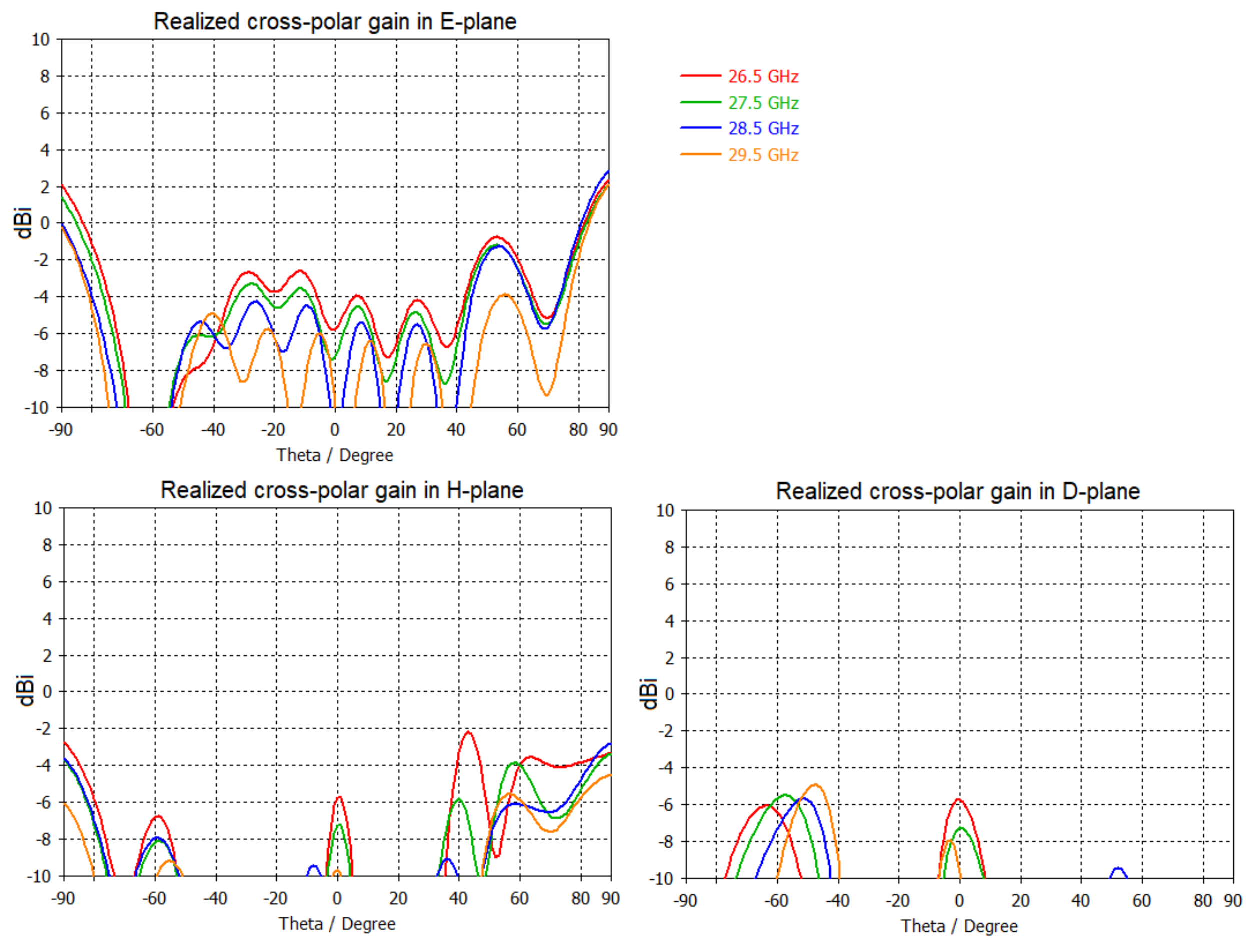

Figure 20: Cross-polar gain of design 1 element embedded on the side of an array

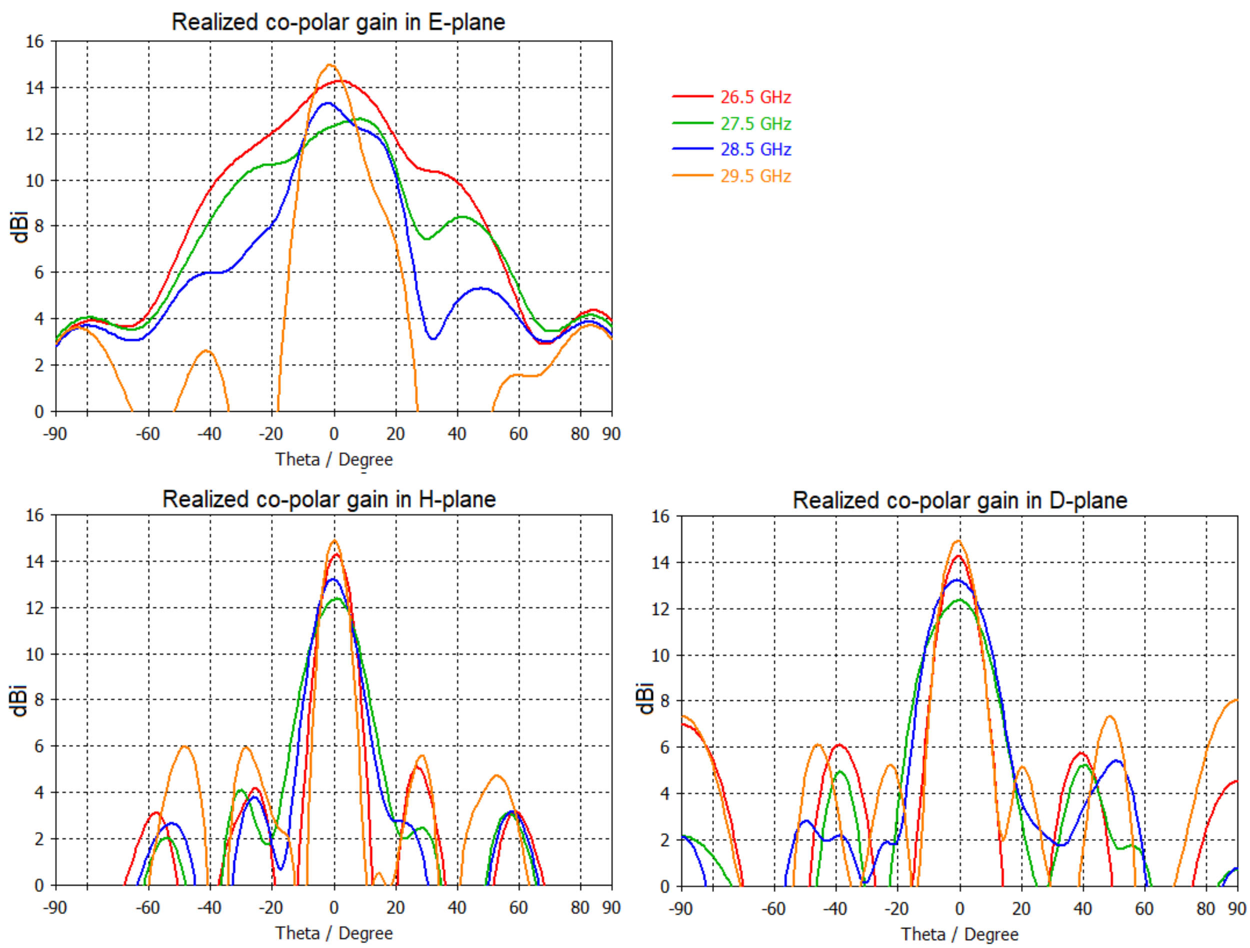

Figure 21: Co-polar gain of design 1 element embedded in the center of an array

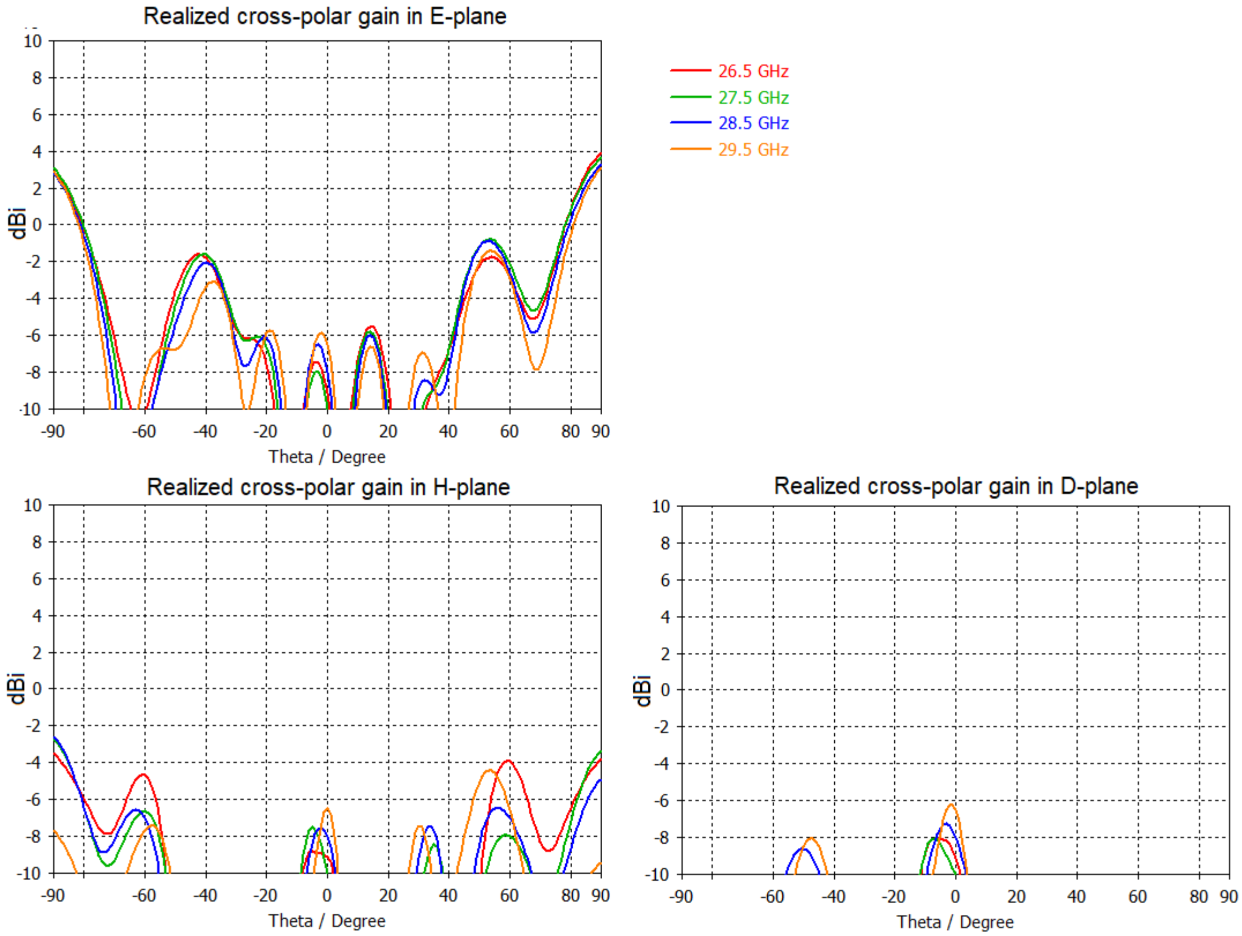

Figure 22: Cross-polar gain of design 1 element embedded in the center of an array

In figure 23 the mutual coupling between several elements in the four-element array is shown. Not all combinations are given as they are equal to the ones already shown due to symmetry. The mutual coupling does not exceed the -20 dB and therefore meets the requirements.

In figure 24 the reflection coefficient of the four elements is given. It can be seen that the reflection coefficient of element 1 and 4 and element 2 and 3 are equal. The reflection coefficient is for a part of the frequency band slightly worse than the required -10 dB, with a maximum of -9 dB.

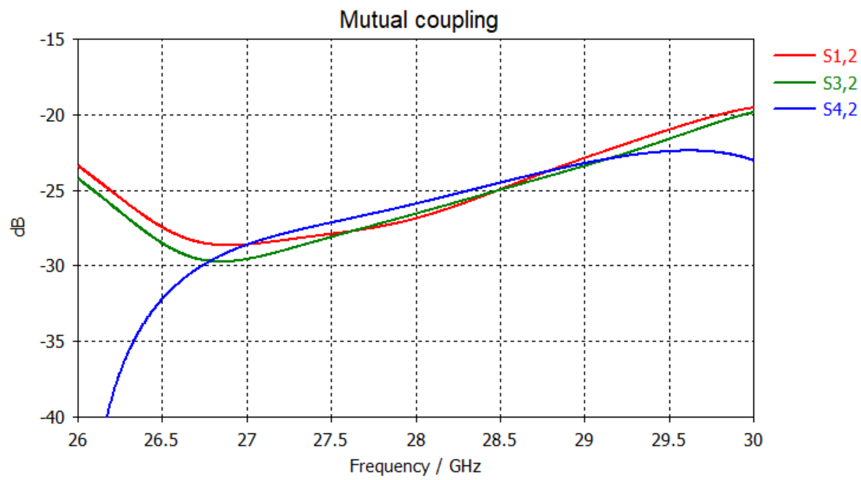

Figure 23: Mutual coupling between elements of a design 1 array

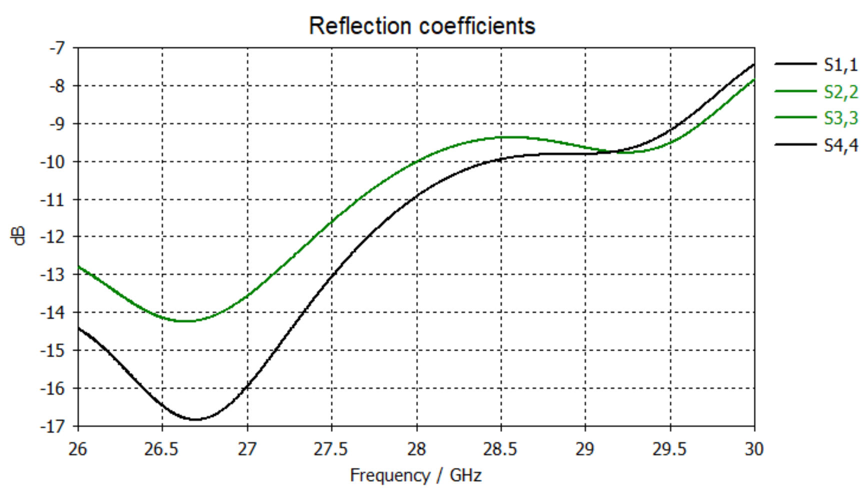

Figure 24: Reflection coefficient of the different elements of a design 1 array

In figure 25 the maximum realized co-polar gain over frequency is shown for all four elements. Again, the results from element 1 and 4 and element 2 and 3 are equal due to symmetry. The realized gain for the center elements is lower than for the edge elements, which can be partly explained by the higher reflection coefficient.

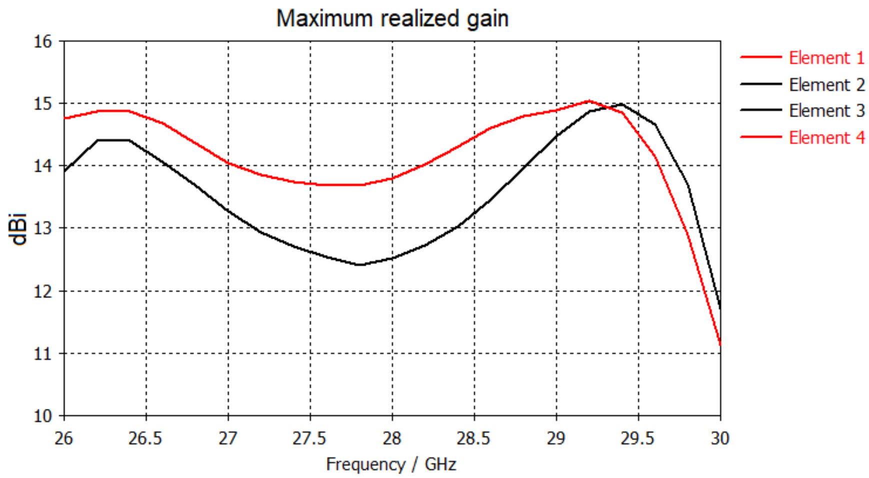

Figure 25: Maximum realized co-polar gain of the different elements of a design 1 array

4.2.4 Array antenna results

In this section the results on the phased array of design 1 are given. In figure 26 the realized co-polarization gain patterns are given for the E- H- and D-plane. In the H-plane side lobes up to 12 dB can be seen. The sidelobe level here is only 8 dB which is lower than the wanted 10 dB. Furthermore it can be seen that the gain of the main lobe is between 18 and 20 dB. This is around 6 dB higher than for the single element, as can be expected from quadrupling the amount of active elements.

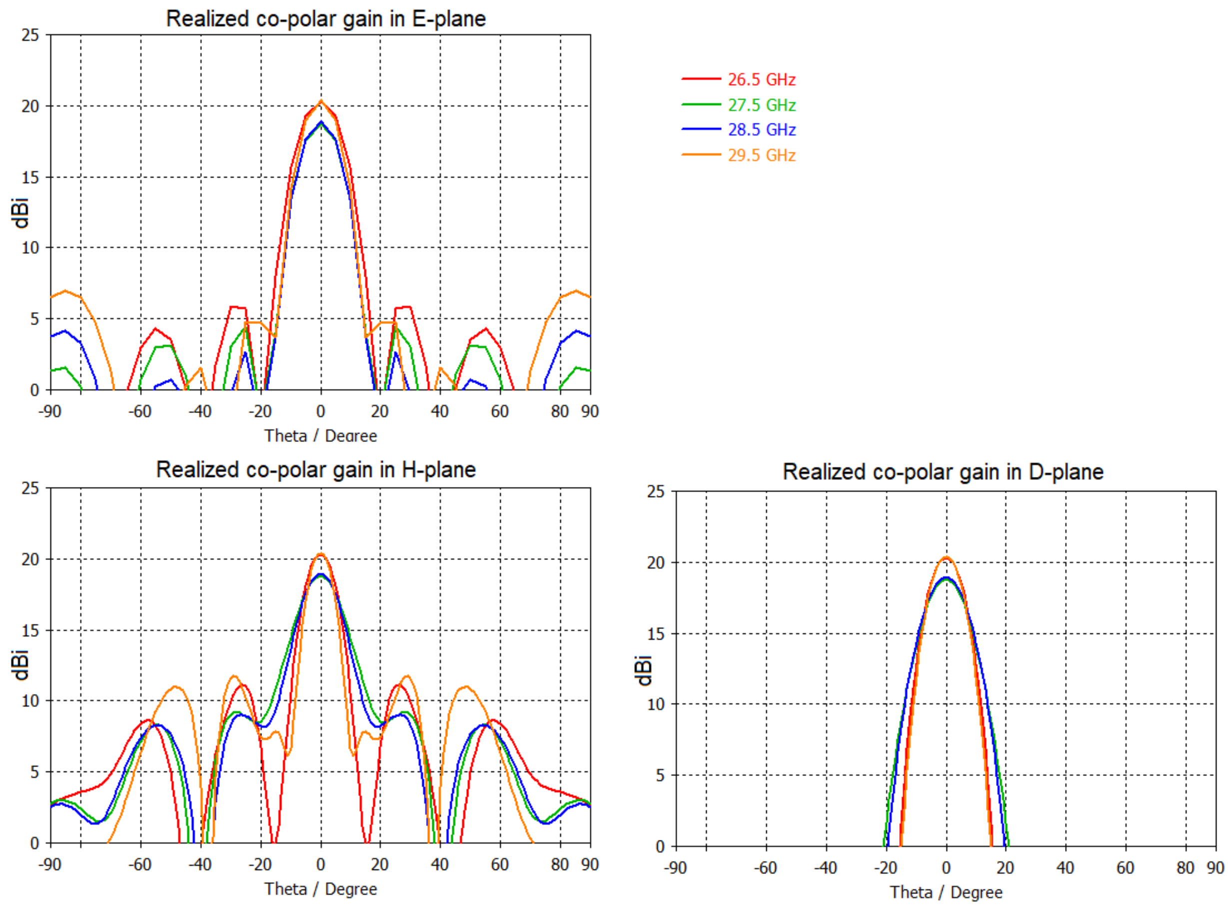

Figure 26: Realized co-polar gain of design 1 phased array with 0° scan angle

In figure 27 the realized cross-polarization gain patterns are given for the E- H- and D-plane. This cross-polarization gain is mostly below 0 dB, especially when only looking at an angle of -45 to 45 degree. The cross-polarization ratio is therefore at least 20 dB, which satisfies the requirements.

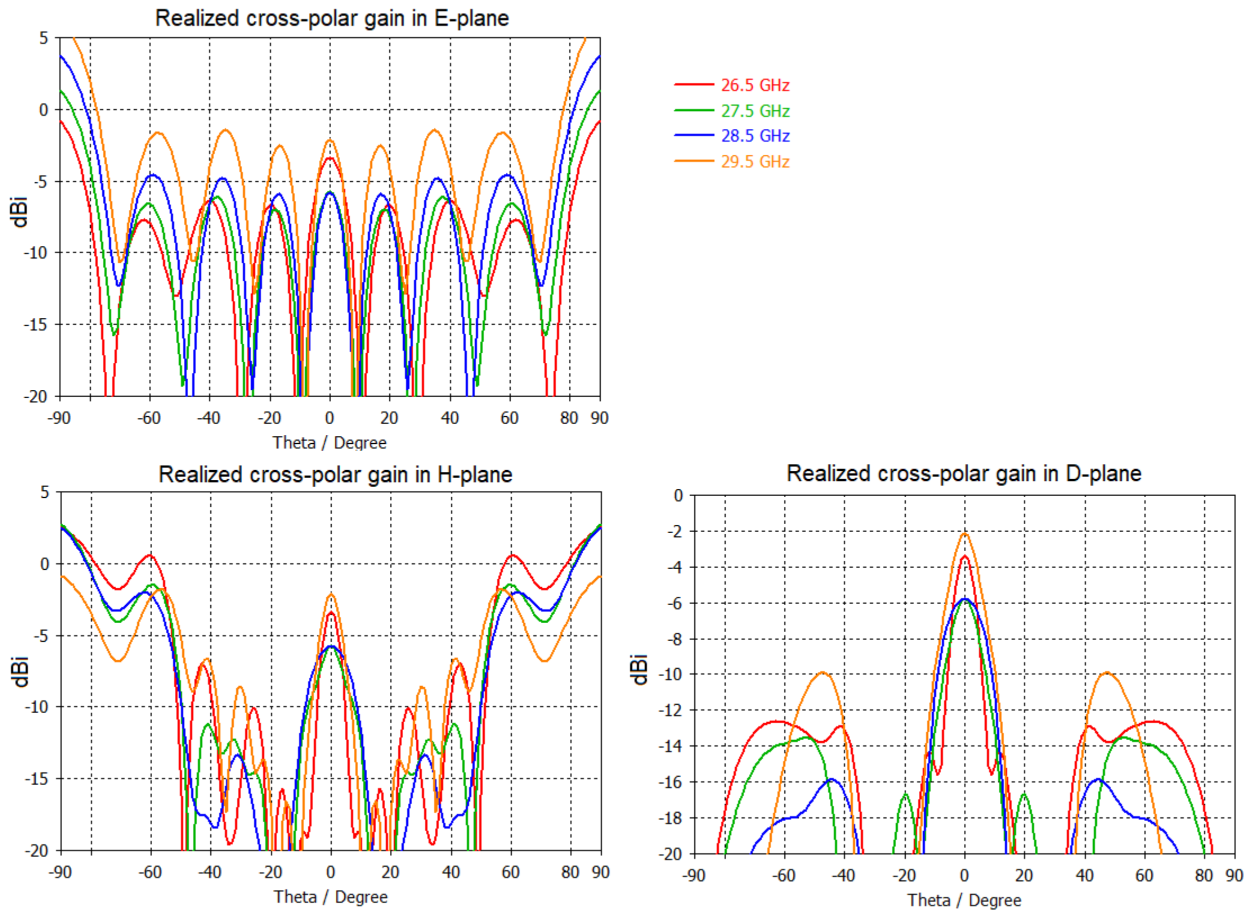

Figure 27: Realized cross-polar gain of design 1 phased array with 0° scan angle

In figure 28 the active reflection coefficients (ARC) for the four elements in the phased array are shown. Within the frequency range of interest the ARC is mainly below the required -10 dB, with a maximum of -9 dB.

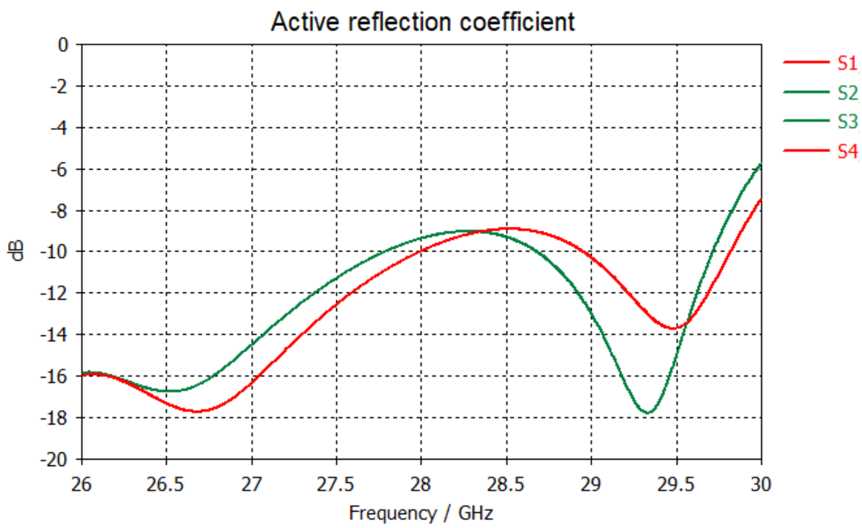

Figure 28: Active reflection coefficient of design 1 phased array with 0° steering angle

In figure 29 the realized co-polarization gain patterns in the E-plane are given for different scanning angles. From these results it can be seen clearly that the gain degrades for increasing scanning angles, especially at higher frequencies. At 29.5 GHz for example, the 15° scanning angle has already decreased with more than 5 dB compared to 0°. Another important issue is the presence of large side lobes. At 26.5 GHz for example, the side lobes at 30° and 45° are already comparable in gain to the main lobe. These grating lobes are present due to the large distance between the elements of 0.822 λ, which is larger than the maximum allowed 0.58 λ calculated in equation 2. With this equation it can be calculated that for a 0.822 λ distance a maximum scan angle of only 12.5° can be reached without grating lobes.

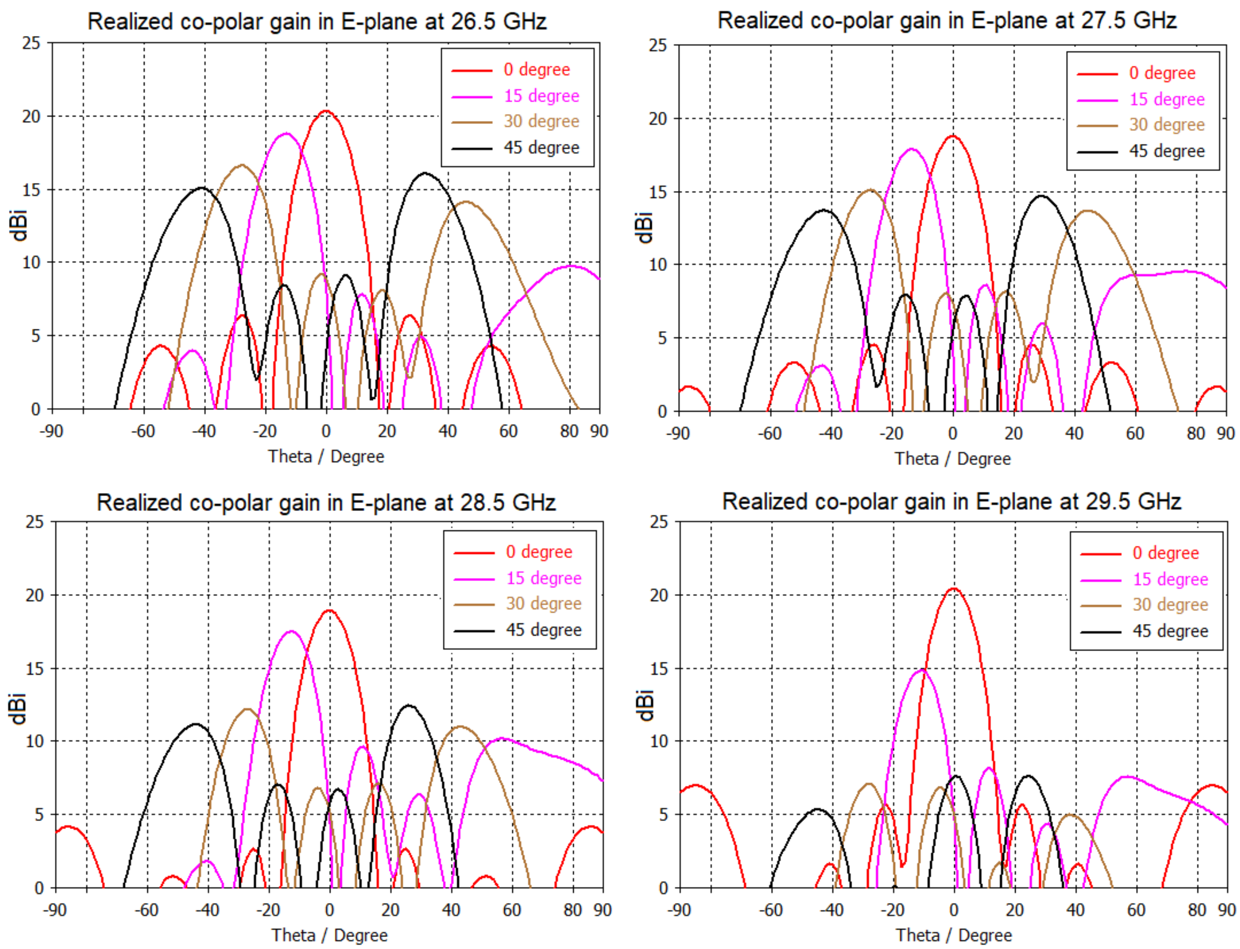

Figure 29: Realized co-polar gain of design 1 phased array for different scanning angles

In figure 30 and 31 the maximum realized co-polar gain and total efficiency of the phased array are shown respectively. From the maximum gain it is again visible that the gain degrades for increasing scanning angles, reaching levels that are far from useful. The total efficiency however, is above the -1 dB up to 29.5 GHz and therefore meets the requirements.

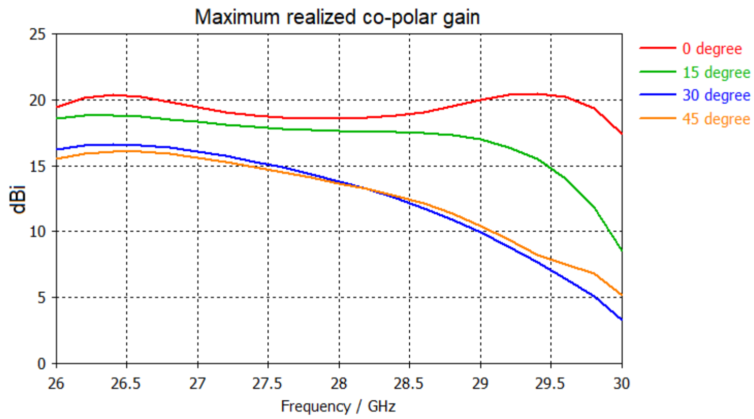

Figure 30: Maximum realized co-polar gain of design 1 phased array for different scanning angles

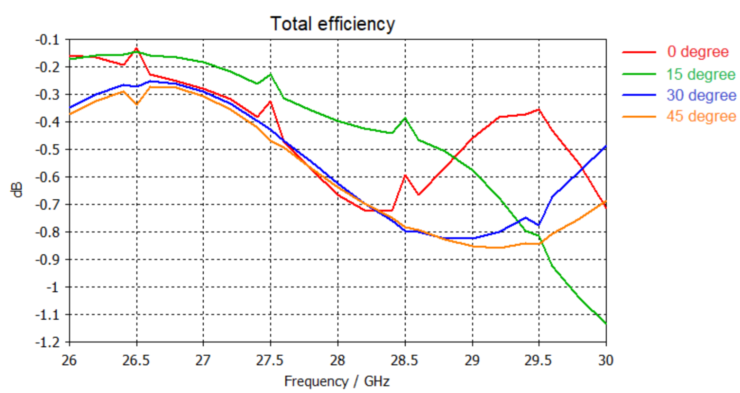

Figure 31: Total efficiency of design 1 phased array for different scanning angles

4.3 Design 2

In this chapter the results on design 2 will be given and commented on. First the designed model is given for both single element and an array. Then the results are given for a single element in free space, on the edge and in the center of an array, respectively. Next, the results on a 4-element phased array as a whole are given, and in the last part the results on a 8-element phased array are given.

4.3.1 Design models

The CST model of a single element of design 2 can be found in figure 32. The gap between the distribution layer and radiation layer in the top picture has been overdrawn for visual purposes. The exact parameters can be found in table 2.

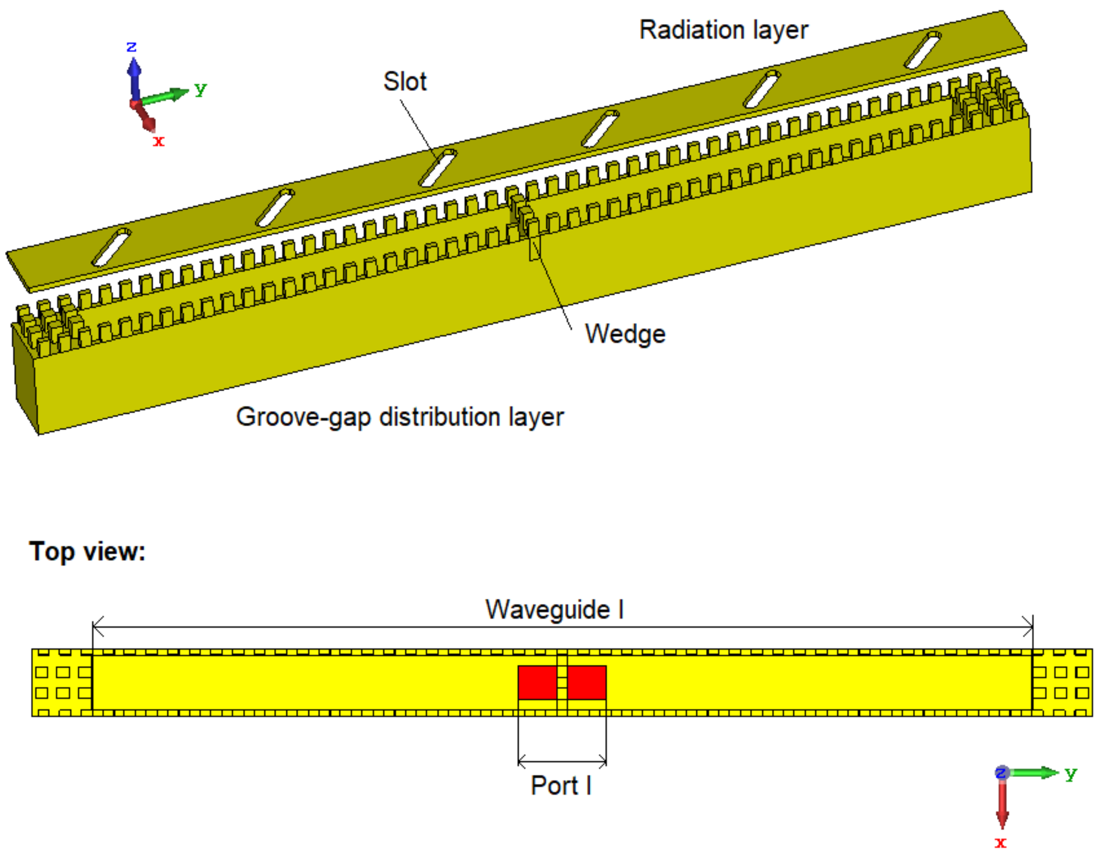

Figure 32: CST model of a single element of design 2

The CST model of the phased array of design 2 is shown in figure 33. The baffles are shown, and also the $\pm 7.0mm$ shift in the y direction of every element is visible. All design parameters from table 2 are still valid. The 8-element array is two times the 4-element array placed directly next to each other.

Parameter	Size (mm)	Description
Pin_h	1.5	Height of the pins
Pin_w	0.9	Width of the pins
Pin_t	0.85	Space between pins
$Waveguide_w$	4.5	Width of the waveguide (between the pins)
$Waveguide_h$	8.5	Height of the waveguide (Pin_h)
$Waveguide_l$	77.1	Length of the waveguide (between the pins)
$Slot_w$	1.2	Width of the slots
$Slot_l$	5.6	Length of the slots
$Blend_r$	0.5	Blend radius of slot corners
$Slotdisty$	14.0	Spacing between the slots y-axis
$Slotdistx$	0.0	Displacement in +x or -x for every other slot
$Port_l$	7.2	Length of the port in bottom plate
$Port_w$	2.8	Width of the port in bottom plate
$Wedge_w$	0.9	Width of the wedge (equal to pin_w)
$Wedge_h$	3.7	Height of the wedge (down from top plate)
$Baffle_w$	1.2	Width of the baffles (array only)
$Baffle_h$	3.3	Height of the baffles (array only)

Table 2: Parameter table Design 2

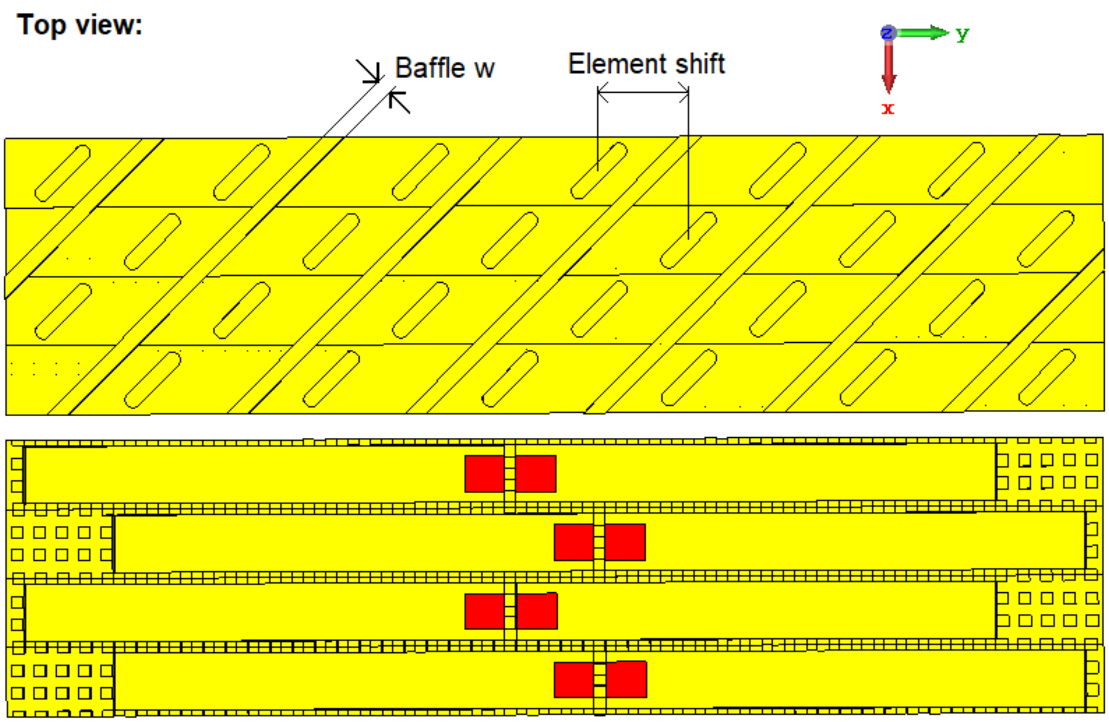

Figure 33: CST model of 4-element phased array of design 2

4.3.2 Single element results

First, the results on a single element in free space are given. The co-polar and cross-polar gain in the E-, H- and D-plane can be found in figure 34 and 35 respectively.

An important observation from these results is the large side lobes in the H-plane and D-plane. These grating lobes occur due to the distance between the slots being greater than one wavelength, as explained in chapter 2.3.3. Another observation is the large reduction in gain at 29.5 GHz. It should however be noticed that the dimensions used in the model have been optimised for the final phased array including baffles, which might not be optimal for a free space element without baffles.

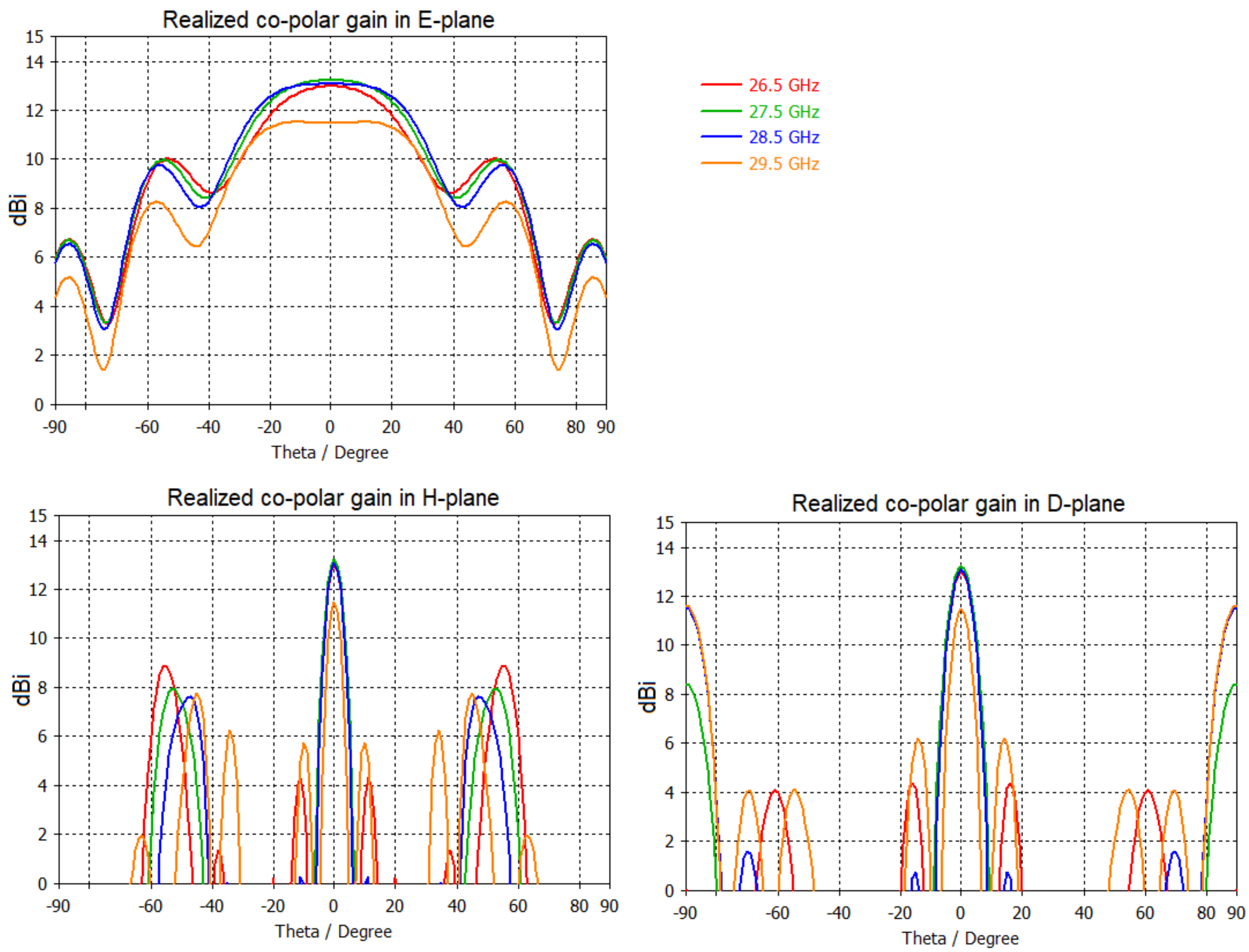

Figure 34: Co-polar gain of single element in free space of design 2

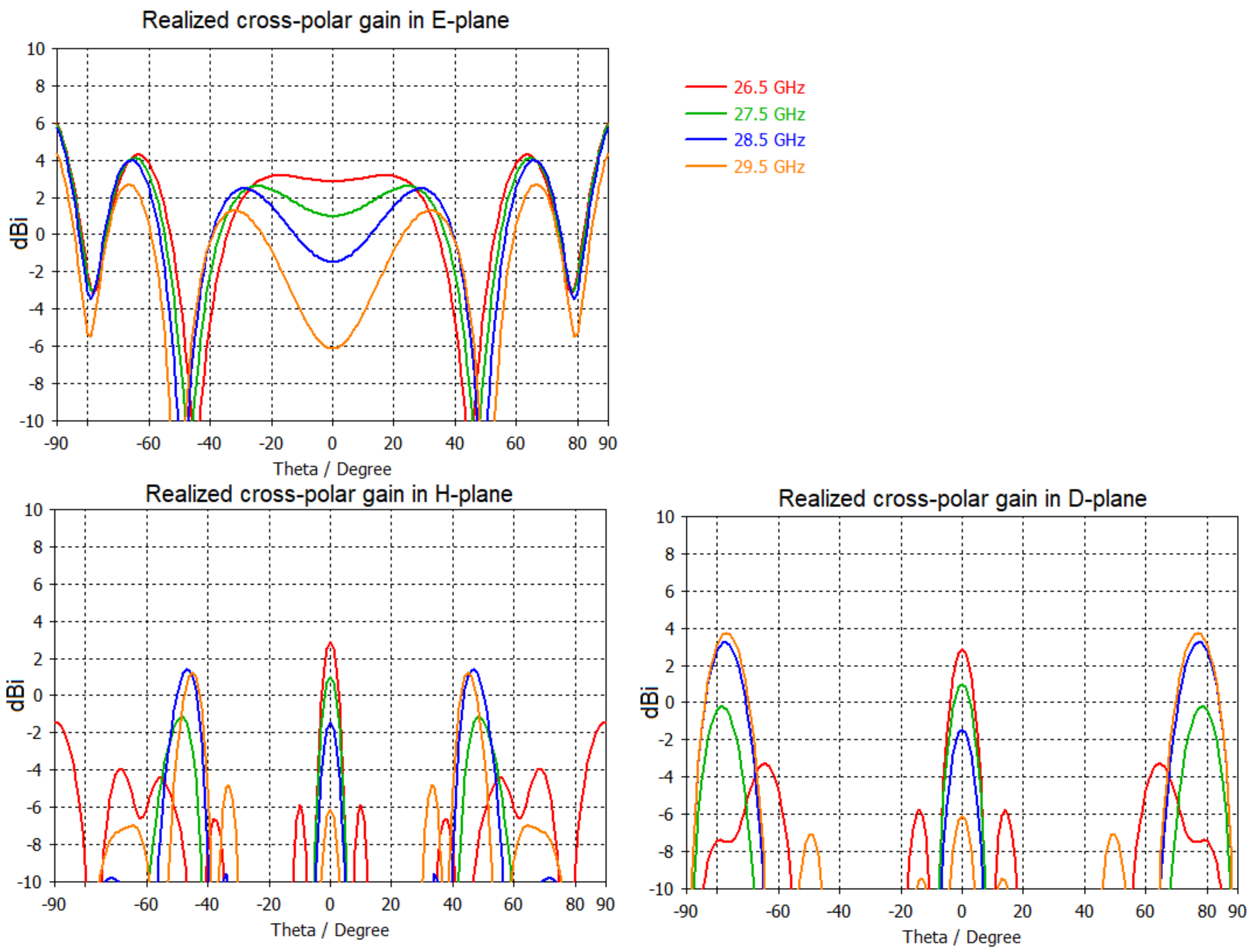

Figure 35: Cross-polar gain of free space element of design 2

In figure 36 the reflection coefficient of the single element is shown. A steep increase at the higher frequencies can be observed, which can also explain the reduction of realized gain at 29.5 GHz discussed above. In figure 37, the maximum realized gain as a function of frequency is shown. Here the reduction of gain for higher frequencies as a result of increasing reflection is clearly visible.

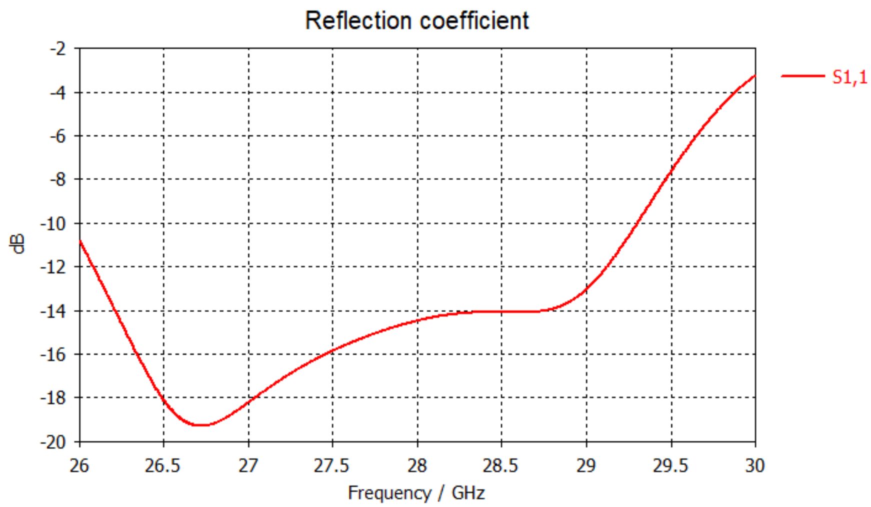

Figure 36: Reflection coefficient of single element in free space of design 2

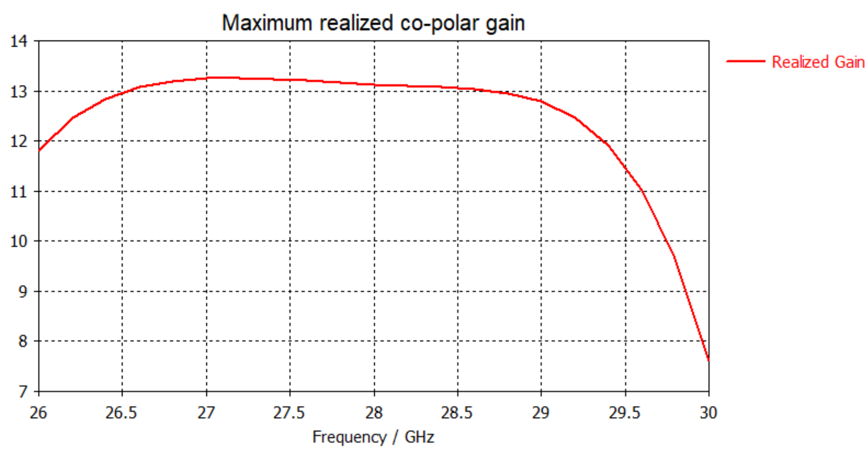

Figure 37: Maximum realized co-polar gain of single element in free space of design 2

4.3.3 Embedded element results

Next, the results on a single element on the side of a four-element array is given. Because the final array includes baffles, they are already included in the model. The co-polar and cross-polar gain in the E-, H- and D-plane can be found in figure 38 and 39 respectively.

Again large grating lobes are visible in the H-plane. This should however not form a problem for the array as a whole as the shift between the elements in the y-direction will result in destructive interference for these side lobes. The grating lobes in the D-plane, that cannot be solved by this shift have already been reduced by the baffles, and are therefore no longer a problem.

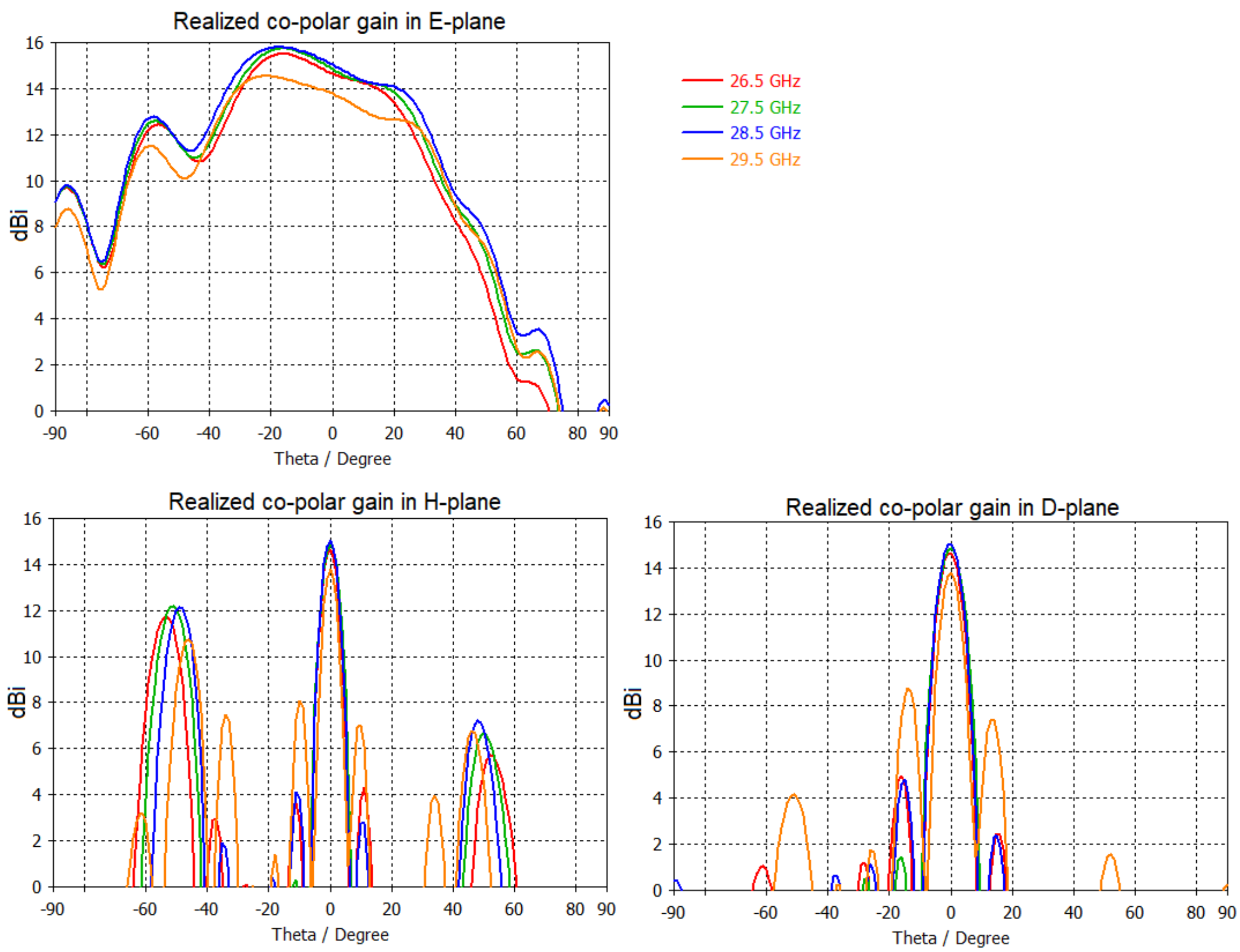

Figure 38: Co-polar gain of design 2 element embedded on the side of an array

From figure 39 it can be seen that the cross-polarization gain in the H- and D-plane have reduced compared to the free space element without baffles. The cross-polarization gain in the E-plane however is still quite large, with values up to 4 dBi at small angles, and up to 8 dBi at large angles.

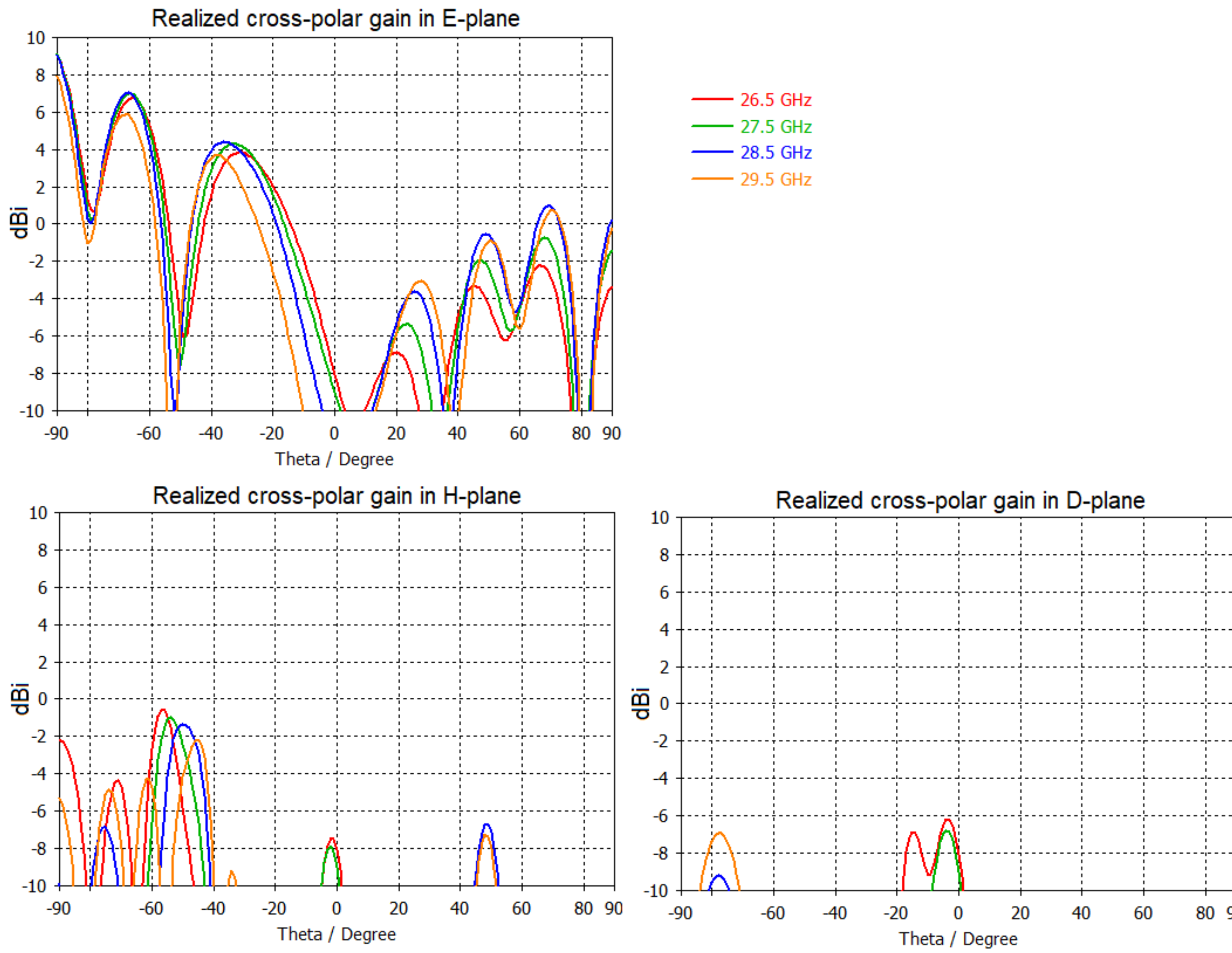

Figure 39: Cross-polar gain of design 2 element embedded on the side of an array

The co- and cross-polar gain for a center element (element 2) are shown in figure 40 and 41.

Comparing the results of the edge and center element it can be seen that the main beam in the E-plane of the edge element is shifted away from the center in the while the main beam of the second element shifted slightly towards the center. The gain in the main beam is also slightly better for the center element, especially for the higher frequency. The results for the cross-polarization do not differ significantly.

Compared to the results from the free space element without baffles, a large reduction in side lobes in the D-plane is visible.

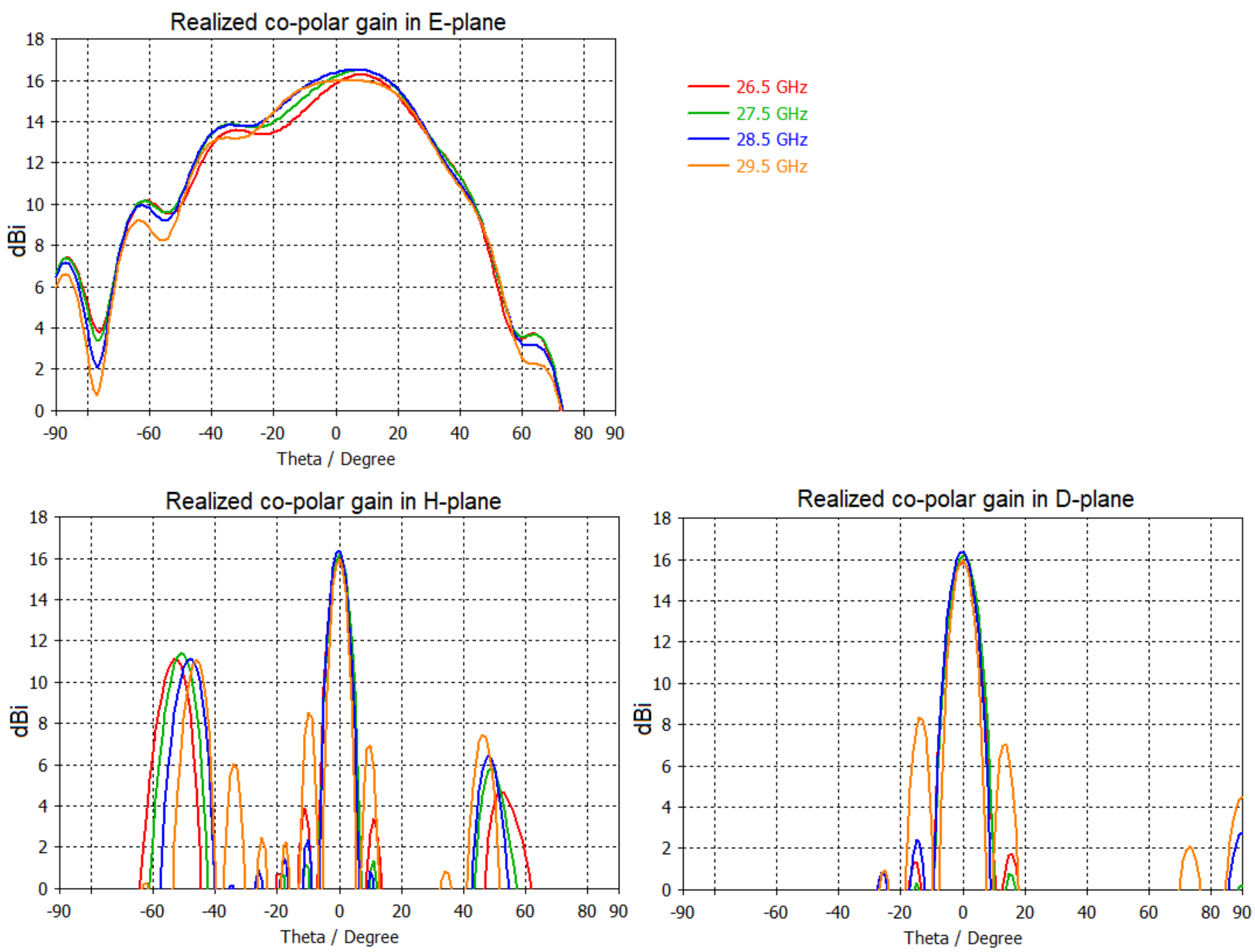

Figure 40: Co-polar gain of design 2 element embedded in the center of an array

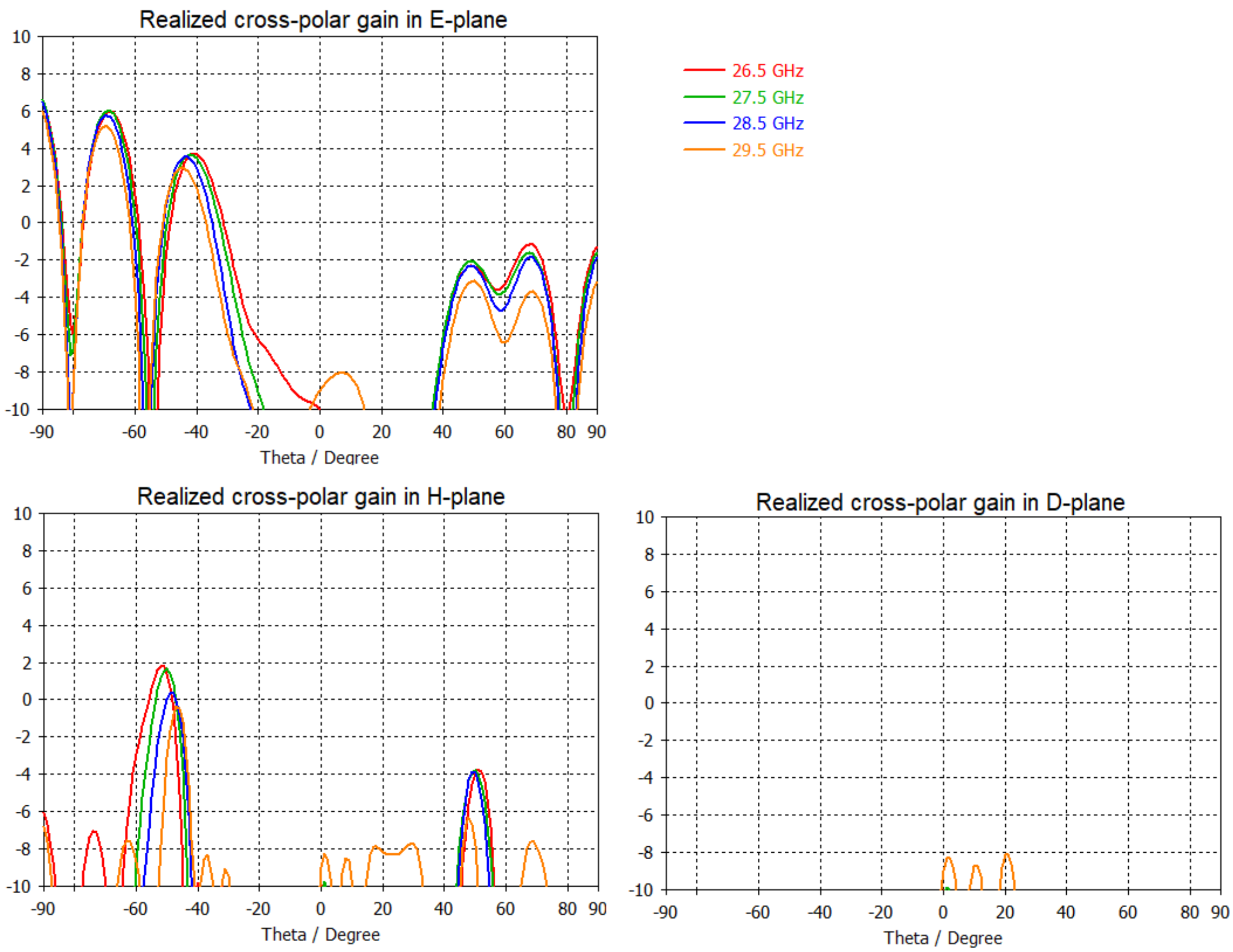

Figure 41: Cross-polar gain of design 2 element embedded in the center of an array

In figure 42 the mutual coupling between several elements in the four-element array is shown. Not all combinations are given as they are similar to the ones already shown. The mutual coupling exceeds the required maximum of -20 dB barely, which is not considered a large problem.

In figure 43 the reflection coefficient of the four elements is given. It can be seen that the reflection coefficient of element 1 and 4 and element 2 and 3 are similar, but not exactly equal. The reflection coefficient of the third element is for a very small part of the frequency band slightly worse than the required -10 dB, with a maximum of -9.5 dB.

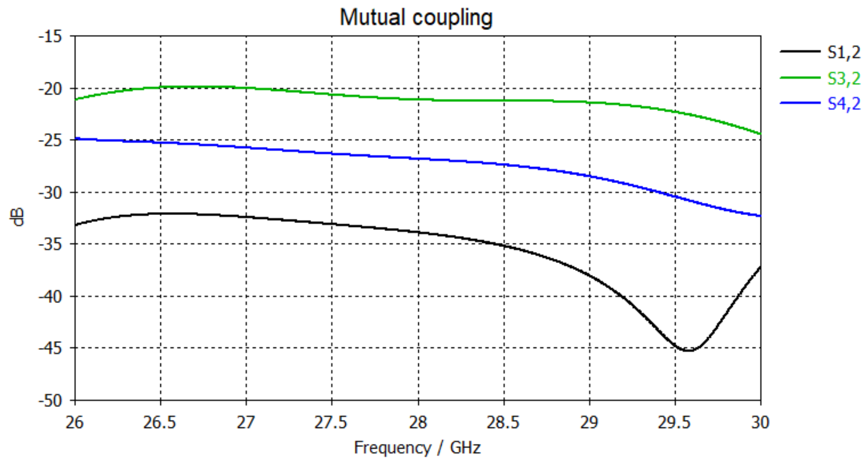

Figure 42: Mutual coupling between elements of a design 2 array

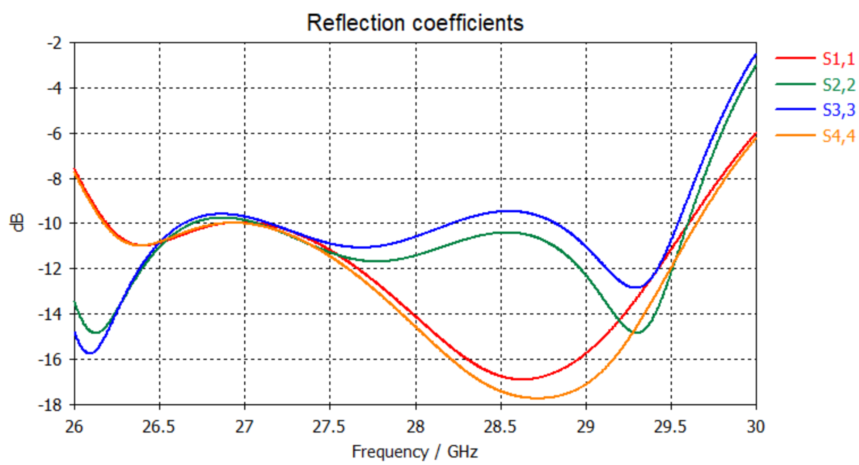

Figure 43: Reflection coefficient of the different elements of a design 2 array

In figure 44 the maximum realized co-polar gain over frequency is shown for all four elements. The realized gain for the center elements is higher than for the edge elements. This is considered positive as the 8-element array will have more elements similar to the center elements.

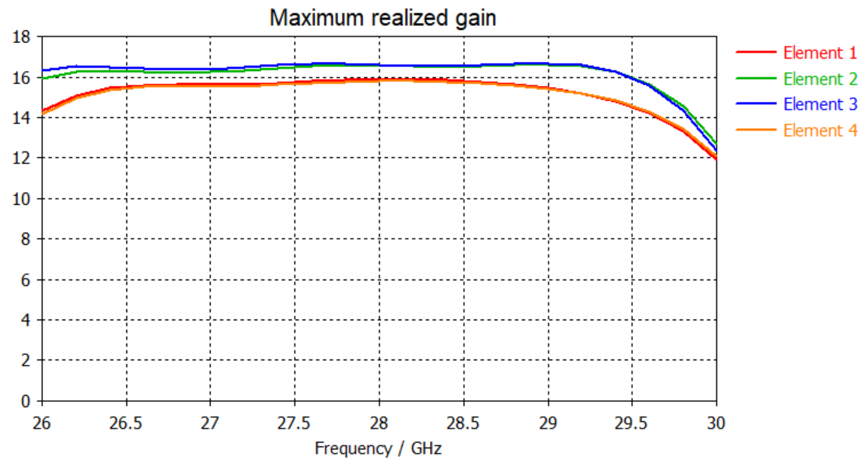

Figure 44: Maximum realized co-polar gain of the different elements of a design 2 array

4.3.4 4-element array antenna results

In this section the results on the 4-element phased array of design 2 are given. In figure 45 the realized co-polarization gain patterns are given for the E- H- and D-plane. The first thing that stands out compared to design 1 is the variation between the frequencies, which is a lot less for design 2. Due to the addition of the baffles, no significant grating lobes are visible. Only in the D-plane a small grating lobe can be spotted at 29.5 GHz, but with a sidelobe level higher than 16 dB this does not pose a problem. Furthermore it can be seen that the gain of the main lobe is between 21 and 22.3 dB. This is around 6 dB higher than for the single element, as can be expected from quadrupling the amount of active elements.

Another important observation is that the large grating lobes in the H-plane around $\pm 60°$ are no longer present due to the destructive interference.

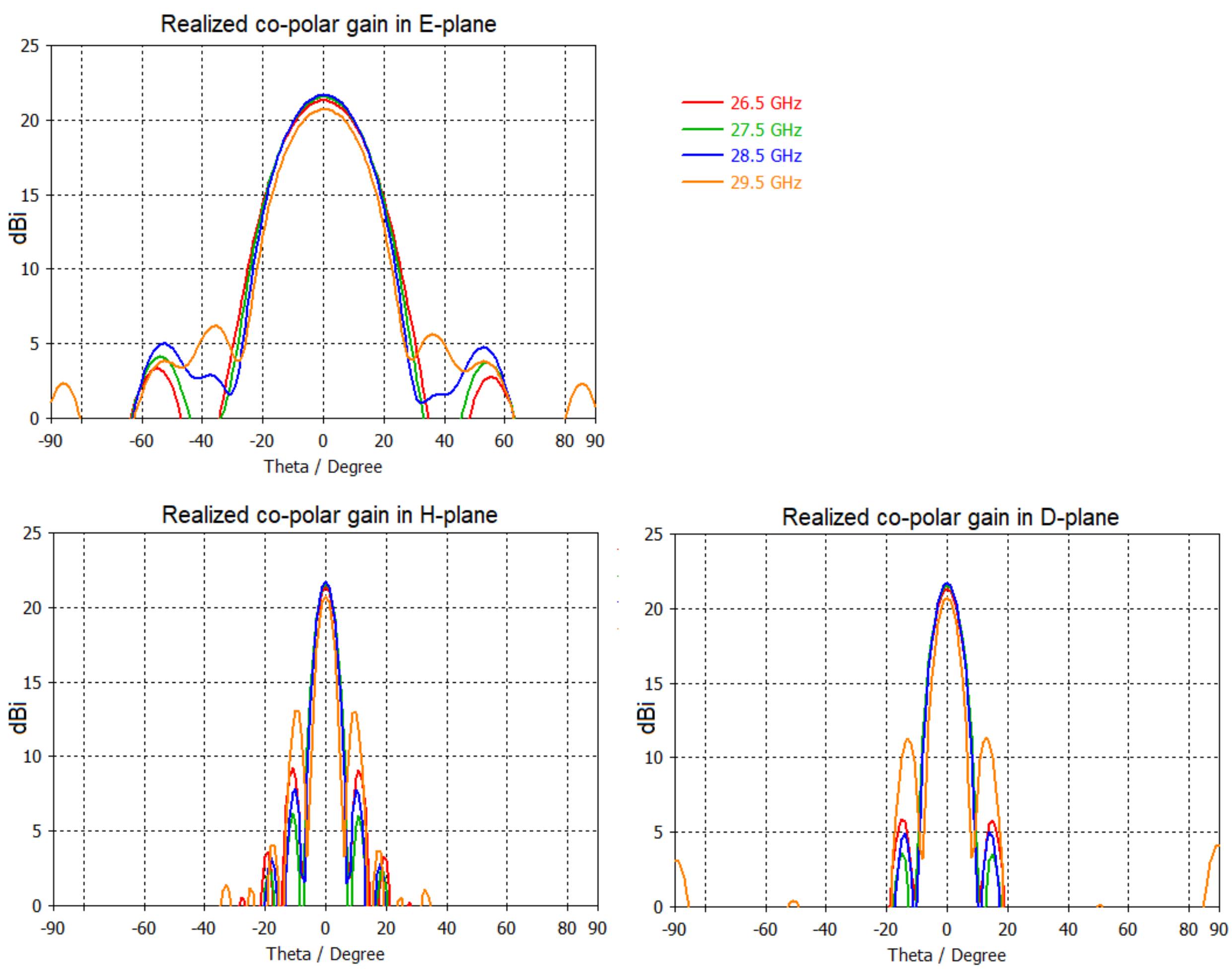

Figure 45: Realized co-polar gain of design 2 phased array with 0° scan angle

In figure 46 the realized cross-polarization gain patterns are given for the E- H- and D-plane. The cross-polarization gain is mostly below 0 dB, only the 29.5 GHz pattern has a few lobes reaching 1 dB. With a co-polar gain more than 21 dB, the cross-polarization ratio is at least 20 dB, which satisfies the requirements.

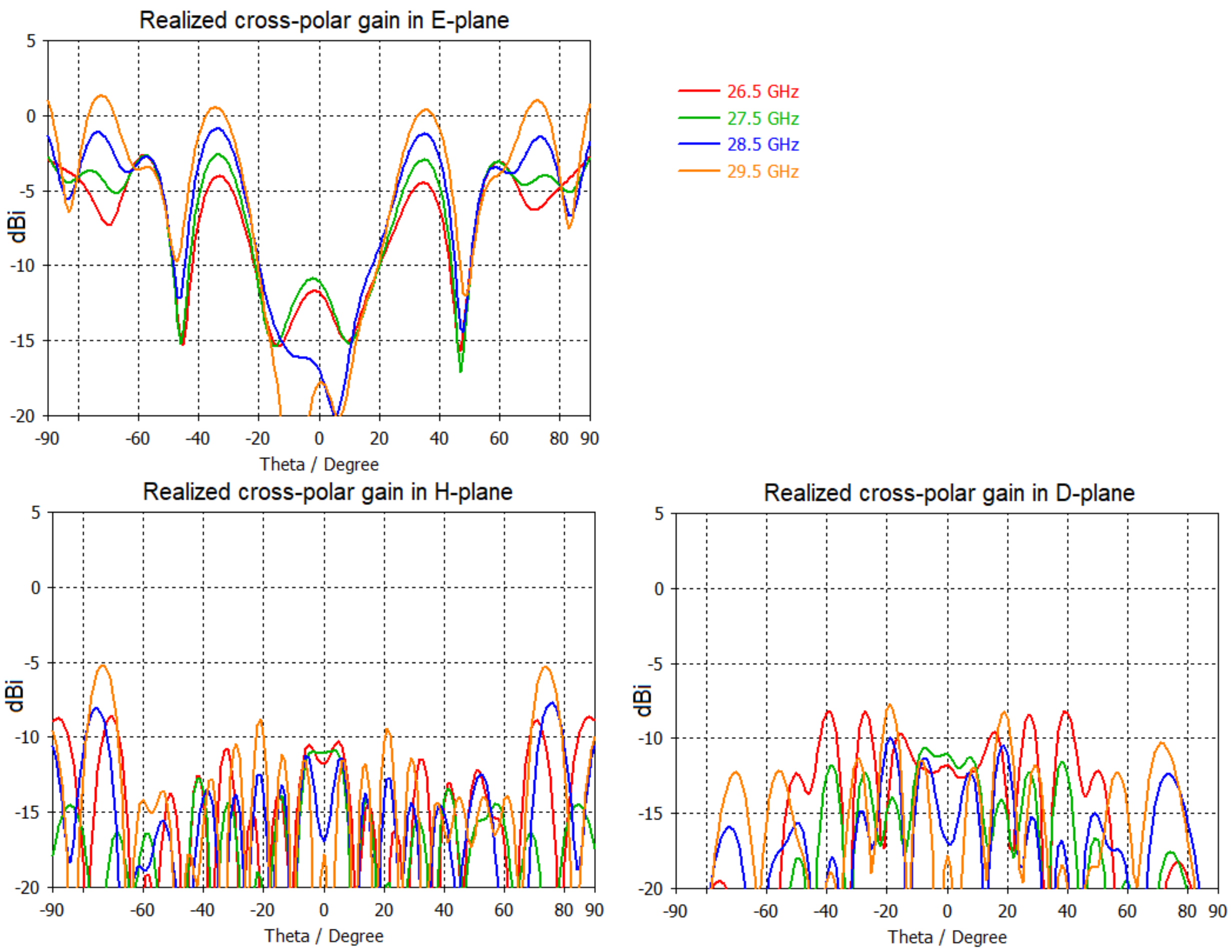

Figure 46: Realized cross-polar gain of design 2 phased array with 0° scan angle

In figure 47 the active reflection coefficients (ARC) for the four elements in the phased array are shown for a 0° scan angle. For the outer two elements the reflection coefficient is not below -10 dB everywhere. The total active reflection coefficient (TARC) of all elements combined however is maximum -11 dB, so as a whole the results are still adequate.

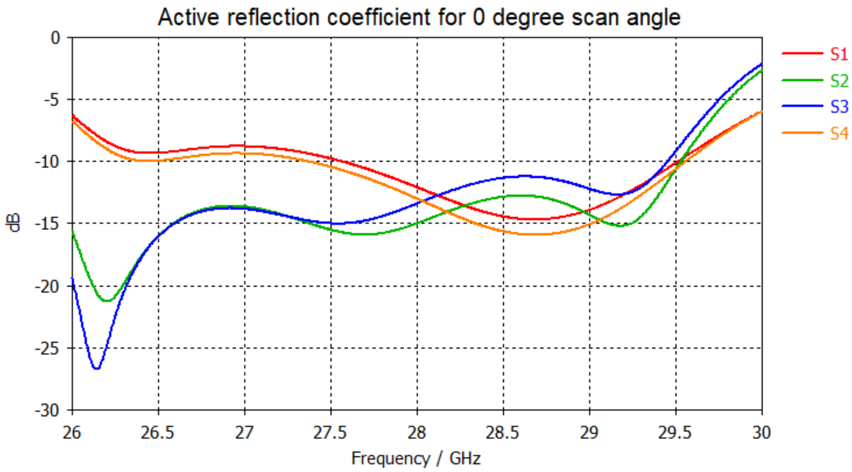

Figure 47: Active reflection coefficient of design 2 phased array with 0° steering angle

In figure 48 the realized co-polarization gain patterns in the E-plane are given for different scanning angles. Again the gain degrades for increasing scanning angles, as expected, but there is little difference between the lower and higher frequencies. Another important observation is the lack of grating lobes. Due to the distance between the elements of 0.5λ being lower than the allowed 0.58λ from equation 2, no grating lobes are present in the E-plane.

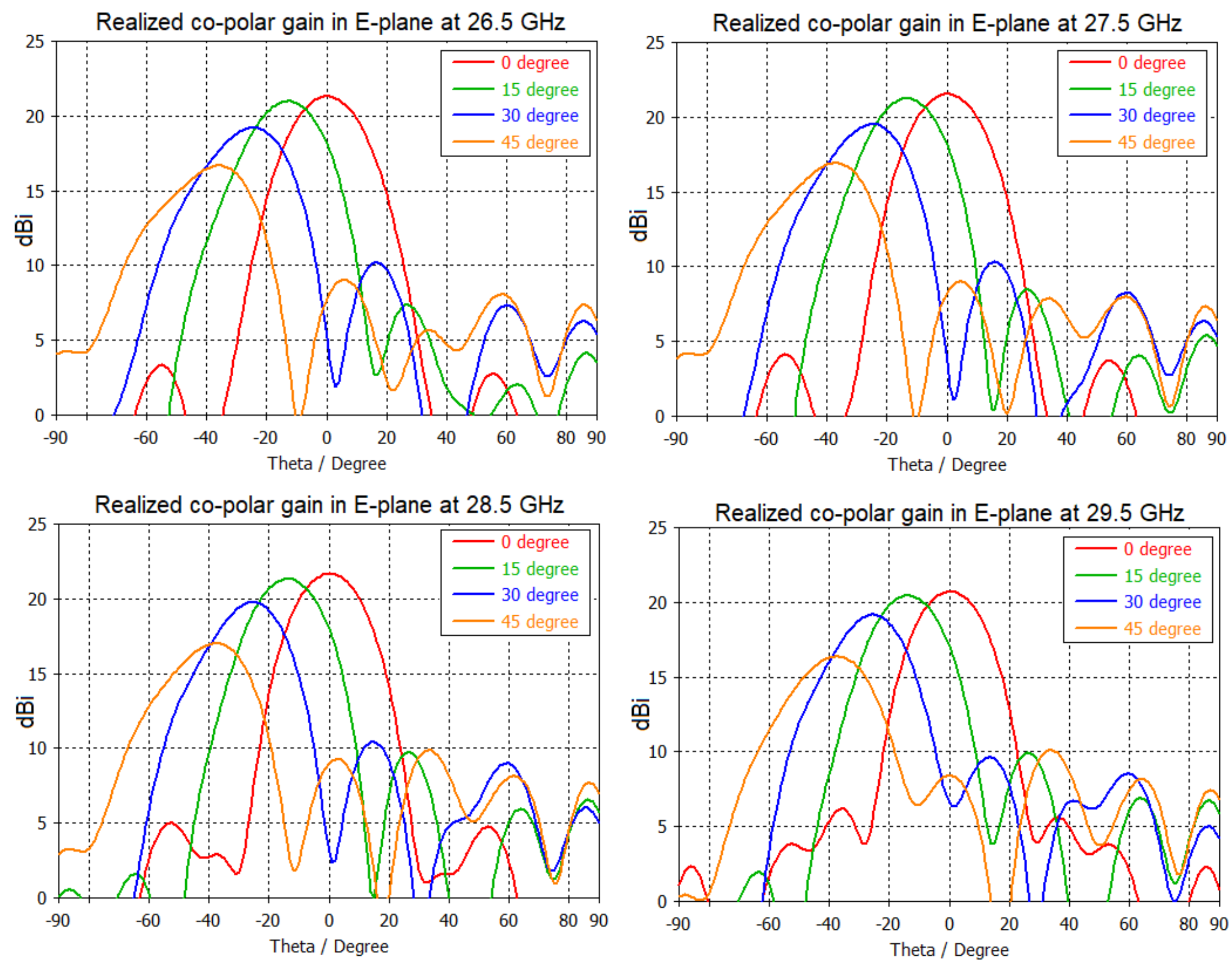

Figure 48: Realized co-polar gain of design 2 phased array for different scanning angles

In figure 49, the ARC for different angles is plotted for element 1 and 3. As expected the ARC changes when the scan angle is changed, but no alarming increase is observed.

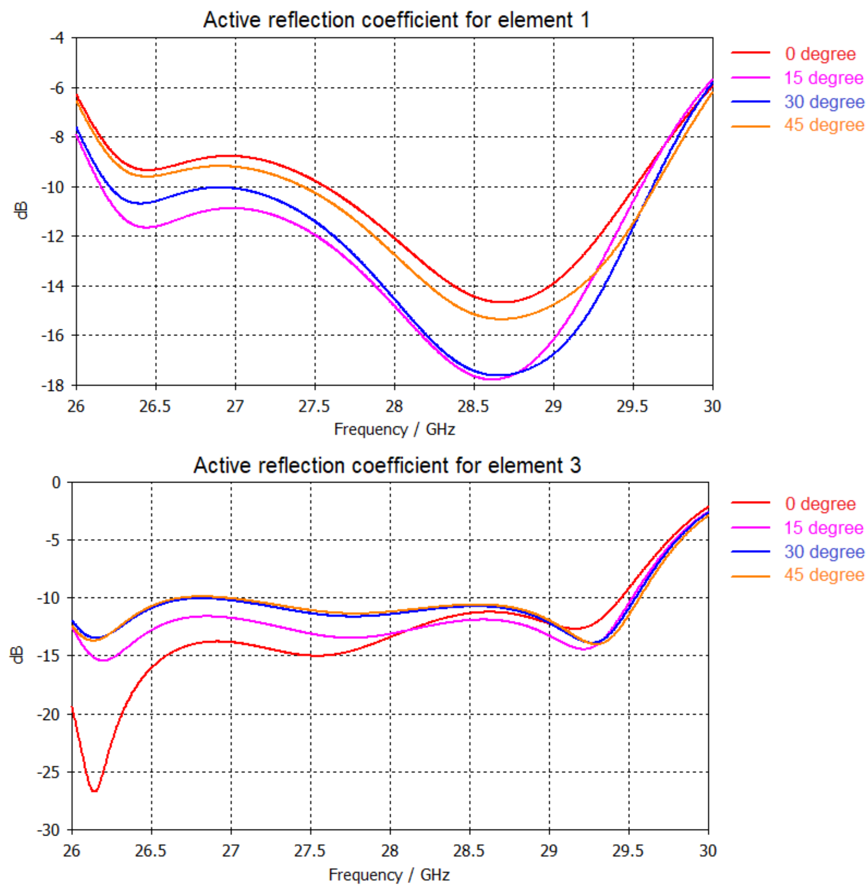

Figure 49: Active reflection coefficient of design 2 phased array for different angles

In figure 50 and 51 the maximum realized co-polar gain and total efficiency of the phased array are shown respectively. It can be seen that for all angles the gain is very flat over frequency. The difference in gain between a 0 and 45 degree scan angle is around 4.5 dB. The total efficiency is, within the frequency range of interest, at least -0.7 dB and therefore meets the required minimum of -1 dB.

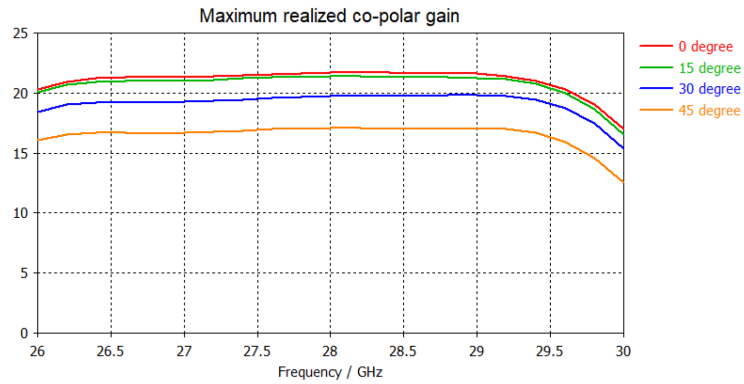

Figure 50: Maximum realized co-polar gain of design 2 phased array for different scanning angles

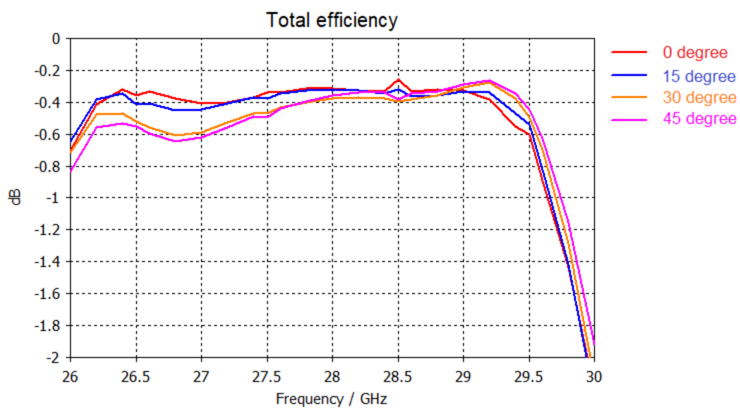

Figure 51: Total efficiency of design 2 phased array for different scanning angles

4.3.5 8-element array antenna results

In this section the results on the 8-element phased array of design 2 are given. In figure 52 the realized co-polarization gain patterns are given for the E- H- and D-plane. With a realized co-polar gain of 24 to 24.7 dB, the gain has increased with approximately 3 dB compared to the 4-element phased array. This 3 dB increase is according to the expectations of doubling the number of elements. The cross-polarization is not plotted since it has barely changed compared to the 4-element results.

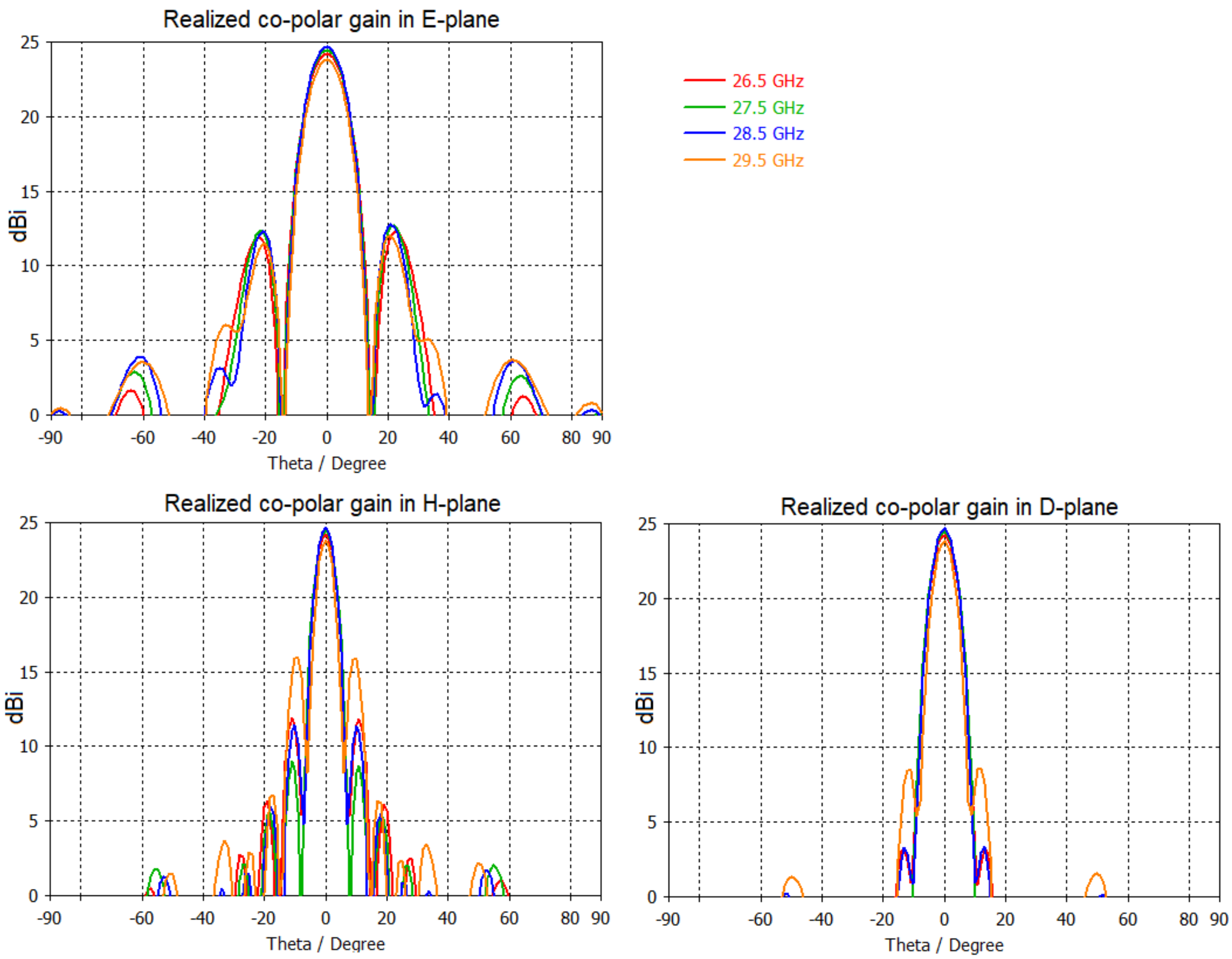

Figure 52: Realized co-polar gain of 8-element phased array with 0° scan angle

In figure 53 the realized co-polarization gain patterns in the E-plane are given for different scanning angles. Apart from the increased gain and the main lobe being smaller, not much difference is visible compared to the 4-element results of figure 48.

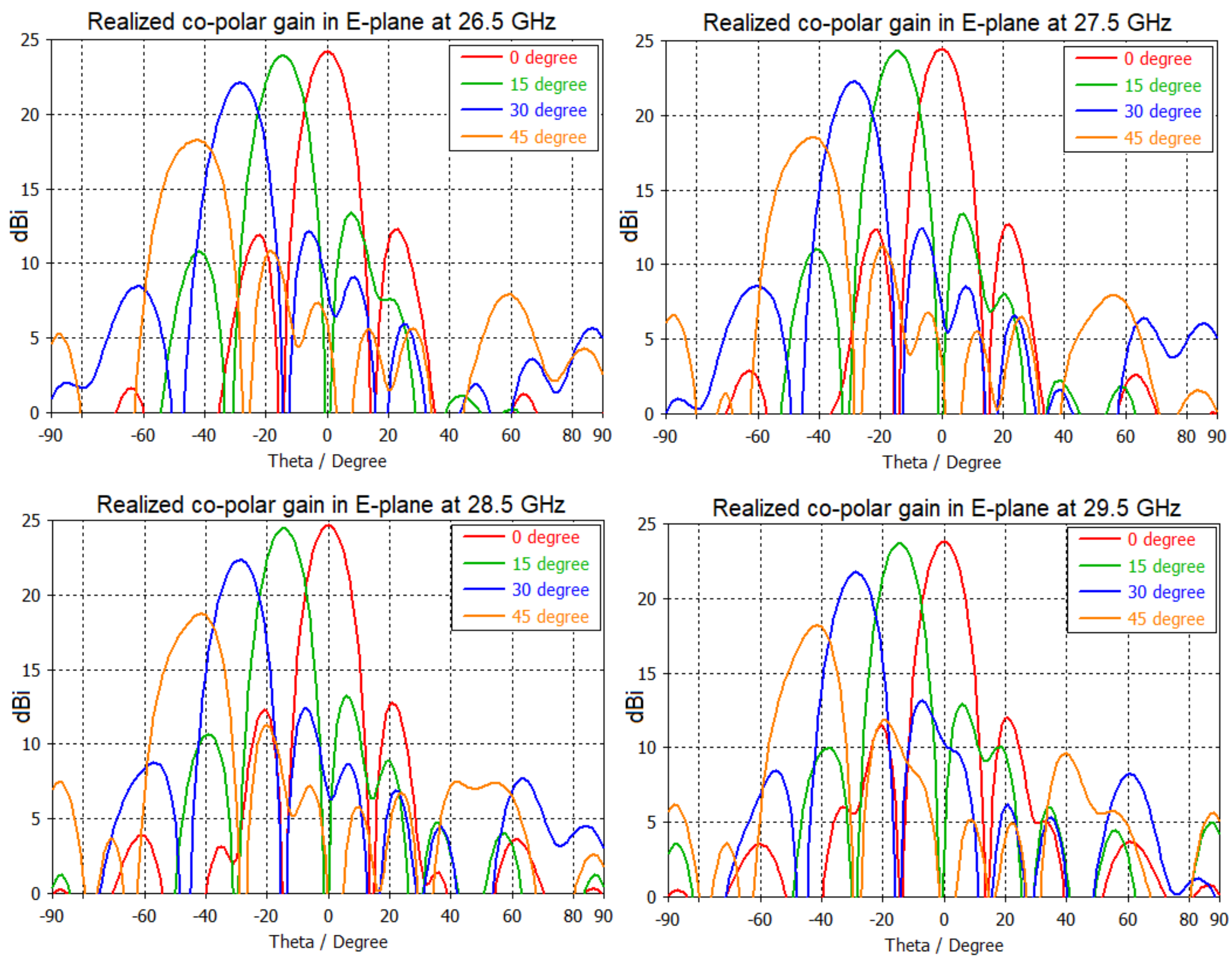

Figure 53: Realized co-polar gain of 8-element phased array for different scanning angles

In figure 54 and 55 the maximum realized co-polar gain and total efficiency of the 8-element phased array are shown respectively. The gain variation over frequency is still very low, as was the case with the 4-element array, and the difference between the gain of different scan angles does not seem to have changed. Furthermore the total efficiency is approximately the same as for the 4-element array plotted in figure 51.

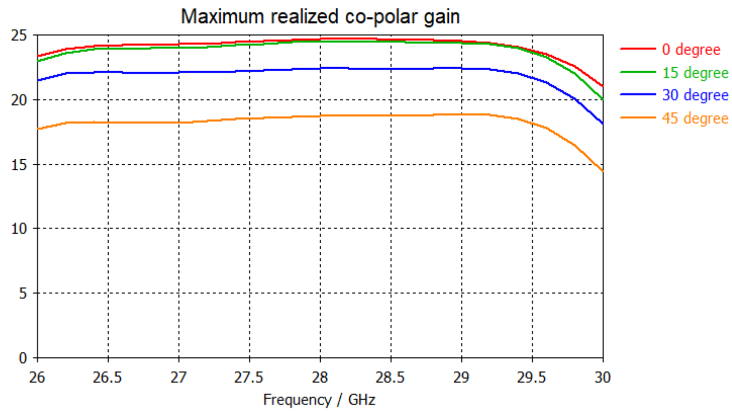

Figure 54: Maximum realized co-polar gain of 8-element phased array for different scanning angles

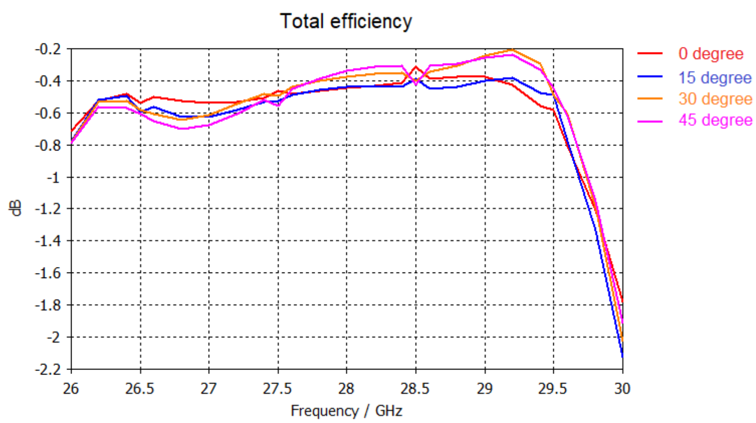

Figure 55: Total efficiency of 8-element phased array for different scanning angles

To make sure there are no hidden side lobes in other planes than the E- H- and D-plane, the UV-pattern is shown in figure 56. From these results it can be seen that larger side lobes are present bottom-right at the 30° scan angles. For the higher frequencies the sidelobe level becomes lower than the preferred 10 dB, up to 6 dB in worst case.

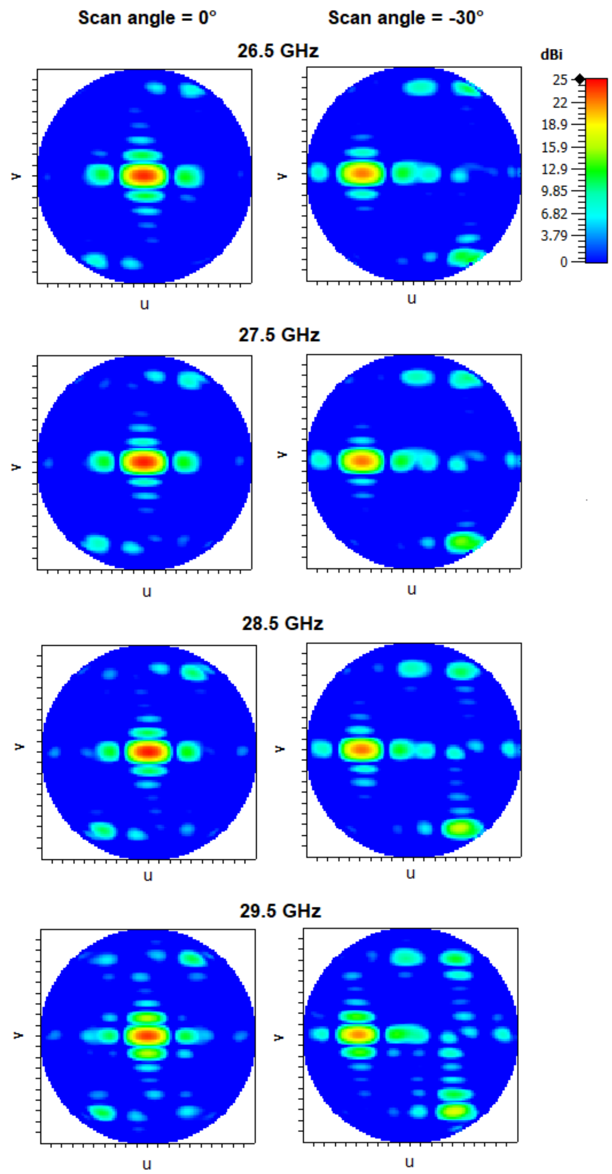

Figure 56: UV-pattern of 8-element array for different frequencies for a 0° and 30° scan angle

4.4 Performance comparison

In this chapter the performance of the designed models is compared to the performance of the existing designs and the requirements. In table 3, an overview is given with all known values for all the designs and the requirements. SIW 1 [3] and SIW 2 [4] are the fixed beam SIW and SIW phased array, and Gap 1 [6] and Gap 2 [7] are the dual polarized gap waveguide and gap waveguide phased array respectively, as mentioned in the introduction. To make a fair comparison between the maximum gain, the gain of the arrays is divided by the number of element in the array. Also the gain per radiation slot has been given.

When comparing the results of design 1 with the requirements it is seen that except for the ARC design 1 meets all the requirements. In the results however it was already shown that design 1 is not suitable as a phased array due to the limited scan angle of 12.5°. Furthermore a significant reduction in gain for higher frequencies was given. This is also visible in the table, as the gain per element is very low compared to other designs.

The results of design 2 are a lot more promising. The only parameter that does not meet the requirements is the ARC. However, as mentioned in the results the TARC does meet this requirement, and therefore it is not considered a problem. Furthermore it can be seen that the gain per element and per slot is the highest of all designs.

	Required	**SIW 1**	**SIW 2**	**Gap 1**	**Gap 2**	**Design 1**	**Design 2**
Type	Gapwave	SIW	SIW	Gapwave	Gapwave	Gapwave	Gapwave
Slanted	Yes	Yes	No	Yes	No	Yes	Yes
Freq. range (GHz)	26.5-29.5		27-29.9	24.25-27.25	26.5-29.5	26.5-29.5	26.5-29.5
Bandwidth (%)	10.7		10.2	11.6	10.7	10.7	10.7
No. of layers	2	2	2	3	2	2	2
0° Average gain		22 dBi	26 dBi	14.5 dBi	23 dBi	19 dBi	24.4 dBi
No. of elements		8	16	1	8	4	8
Gain per element		13 dBi	14 dBi	14.5 dBi	14 dBi	13 dBi	15.4 dBi
Slots per element		7	12	8	8	8	8
Gain per slot		4.5 dBi	3.2 dBi	5.5 dBi	5 dBi	4 dBi	6.4 dBi
ARC	<-10 dB		<-10 dB	<-10 dB	<-10 dB	<-9 dB	<-9 dB
XPR	> 20 dB	25 dB		15 dB		> 20 dB	> 20 dB
Total efficiency	>-1 dB			>-0.5 dB		>-0.8 dB	>-0.7 dB
Mutual coupling	<-20 dB	-33 dB		<-19 dB		<-21 dB	< -20 dB

Table 3: Comparison table

In figure 57, the maximum realized co-polar gain as a function of scan angle is given for design 1 and 2. Here it is also visible that design 1 suffers a lot from grating lobes, lowering the gain of the main beam.

For other existing designs the known data on scan angles is not accurate enough to add to the graphs. However it can be said that the -3dB angle for both SIW 2 and Gap 2 is approximately 45°. For design 2 this -3dB point is at approximately 35°, which is unfortunately 10° less than the two existing designs. This can be explained by the reduction in gain at increasing angles due to the spatial filtering effect of the baffles.

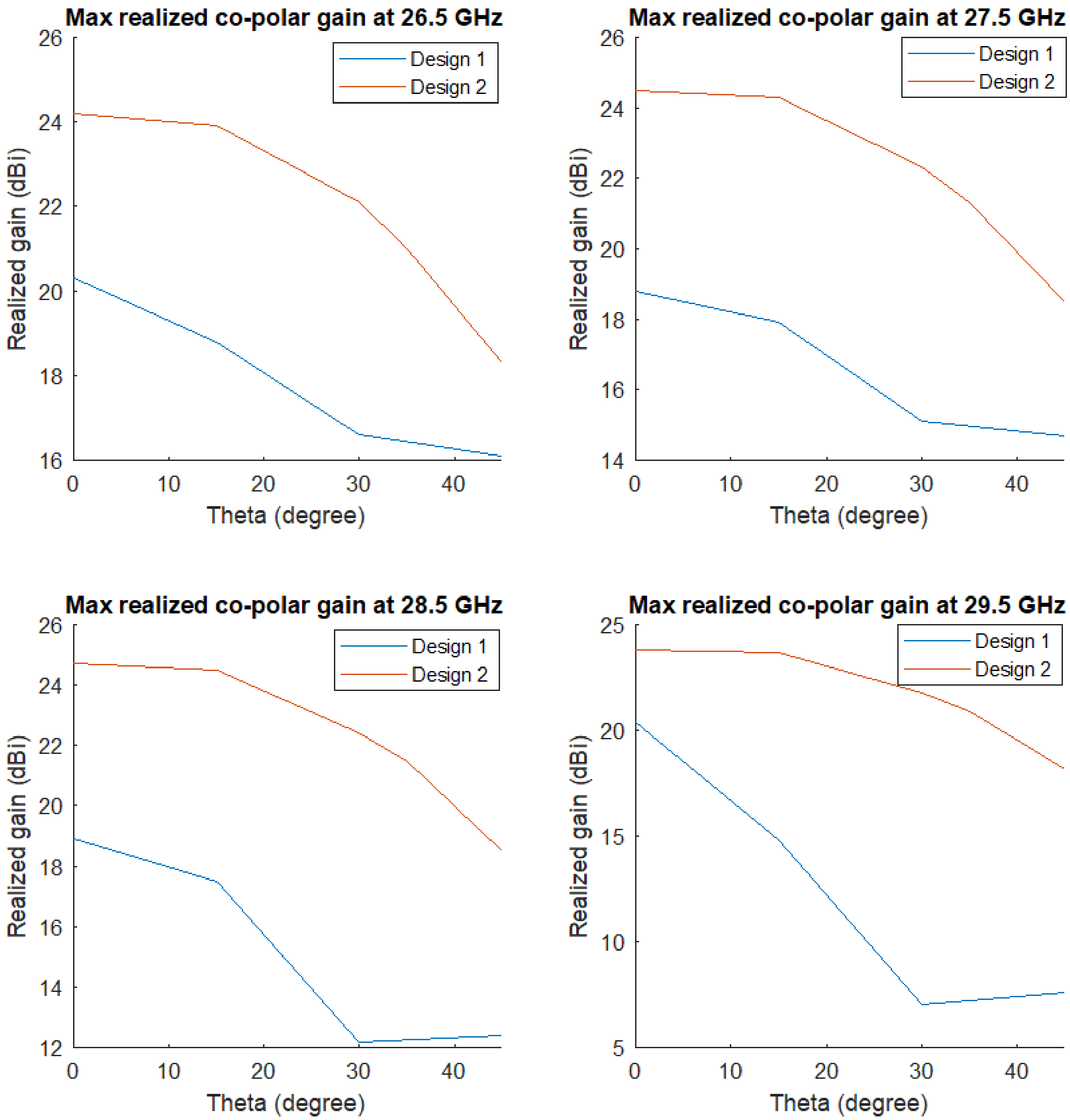

Figure 57: Maximum realized co-polar gain vs scan angle comparison of design 1 and 2

5 Conclusions

In this work an attempt is made to design a 45° slanted slotted waveguide phased array antenna that is both easy to manufacture and without significant loss in gain. The frequency range of this antenna is 26.5 - 29.5 GHz, as this frequency band will be used in multiple countries for 5G. To realize this antenna several design features have been implemented.

Where other antenna designs for this purpose have either a difficult manufacturing process or increased losses due to the presence of a substrate, gap waveguide technology has been used in this antenna design to have a good trade-off between both. Compared to previous gap waveguide designs for this purpose, the number of layers has been reduced from three to two layers to increase manufacturability and therefore decrease costs. Furthermore slots with a 45° slant are used to enable the easy addition of an orthogonal polarization.

The first design that is presented is a horizontal gap waveguide antenna. From the results it can be concluded that the antenna works, but the difference in gain compared to previous designs is deemed too large to be useful. Furthermore the width of the elements is too large, giving a very small look angle of only 12.5° before large grating lobes start to form.

The second design uses a vertical or transversal waveguide which reduces the width and therefore solves the look angle problem of the horizontal waveguide antenna. From the single element results is can be seen that high sidelobes form in the H-plane and with multiple elements also in the D-plane. To reduce these sidelobes a shift of half a wavelength every other element and baffles are used. When combining 8 elements into a phased array, a average realized co-polar gain of 24.4 dBi is reached, which is higher than comparable antenna designs. Furthermore the antenna has a total active reflection coefficient smaller than -10 dB, a total efficiency higher than -0.7 dB and a cross-polarization ratio of at least 20 dB and therefore meets the set requirements. Only the look angle of 45° has not been fully realized as the -3dB point is located around a scan angle of 35°.

With its high realized co-polar gain, cross-polarization ratio and efficiency, this vertical gap waveguide antenna design shows great opportunities in improving performance while keeping the manufacturing costs low.

6 Future work

During this research only simulations have been used to test the performance of the antenna design. Although an attempt was made to make these simulations as realistic as possible, it is still a simulation. A further step would be to realise the design, measure it and if needed optimize it. Furthermore, the layer beneath this antenna that will distribute the signals to the right ports still needs to be developed.

7 References

[1] NXP. *26.5 GHz - 29.5 GHz Quad channel Analog Beam Forming IC*. URL: https://www.nxp.com/products/rf/rf-power/rf-cellular-infrastructure/5g-mmwave/26-5-29-5-ghz-4-channel-analog-beamforming-integrated-circuit:MMW9002KC.

[2] A. Vosoogh, P.-S. Kildal, and V. Vassilev. "Wideband and High-Gain Corporate-Fed Gap Waveguide Slot Array Antenna With ETSI Class II Radiation Pattern in V-band". In: *IEEE Transactions on Antennas and propagation* 65.4 (2017).

[3] S. Park et al. "A Slotted Post-Wall Waveguide Array With Interdigital Structure for 45°Linear and Dual Polarization". In: *IEEE Transactions on Antennas and propagation* 53.9 (2005).

[4] J. Puskely et al. "SIW based antenna array with power equalization in elevation plane for 5G base stations". In: *12th European Conference on Antennas and Propagation (EuCAP 2018)*. 2018, pp. 1–5.

[5] P.-S. Kildal et al. "Local maetamaterial-based waveguides in gaps between parallel metal plates". In: *IEEE Antennas and Wireless Propagation Letters* 8 (2009), pp. 84–87.

[6] A. Bagheri et al. "A ±45° Dual-Polarized Antenna for 5G mmWave Applications Based on Gap Waveguide Technology". In: *2019 International Symposium on Antennas and Propagation (ISAP) IEEE* (2020).

[7] Alireza Bagheri, Carlo Bencivenni, and Andrés Alayón Glazunov. "mmWave Array Antenna based on Gap Waveguide Technology for 5G Applications". In: Sept. 2019, pp. 0492–0494. DOI: 10.1109/ICEAA.2019.8878978.

[8] Rodney G. Vaughan. "Polarization diversity in mobile communications". In: *IEEE Transactions on Vehicular Technology* 39 (1990), pp. 177–186.

[9] B. Lindmark and M. Nilsson. "On the available diversity gain from different dual-polarized antennas". In: *IEEE Journal on Selected Areas in Communications* 19.2 (2001), pp. 287–294.

[10] T. Tomura et al. "A 45° Linearly Polarized Hollow-Waveguide Corporate-Feed Slot Array Antenna in the 60-GHz Band". In: *IEEE Transactions on Antennas and Propagation* 60.8 (2012), pp. 3640–3646.

[11] D. Kim et al. "A Series Slot Array Antenna for 45 °-Inclined Linear Polarization With SIW Technology". In: *IEEE Transactions on Antennas and Propagation* 60.4 (2012), pp. 1785–1795.

[12] Princeton University. *Lecture on beamforming*. URL: https://www.cs.princeton.edu/courses/archive/spring19/cos463/labs/lab5_preview.html.

[13] L. Josefsson. "A grating lobe filter for transverse slot arrays". In: *Antennas and Propagation Society Symposium 1991 Digest*. 1991, 1156–1159 vol.2.

[14] Ashraf Zaman et al. "Overview of High Frequency Electronics Integration Concepts for Gap waveguide based High Gain Slot Antenna Array". In: Nov. 2019, pp. 1–4. DOI: 10.1109/COMCAS44984.2019.8958272.

[15] E. Rajo-Iglesias and P.-S. Kildal. "Groove Gap Waveguide: A Rectangular Waveguide Between Contactless Metal Plates Enabled by Parallel-Plate Cut-Off". In: *Proceedings of the Fourth European Conference on Antennas and Propagation* (2010), pp. 1–4.

[16] P.-S. Kildal et al. "Design and experimental verification of ridge gap waveguide in bed of nails for parallel-plate mode suppression". In: *IET Microwaves, Antennas & Propagation* (2010).

[17] G. Huang et al. "Design of a symmetric rectangular waveguide T-junction with in-phase and unequal power split characteristics". In: *2013 IEEE Antennas and Propagation Society International Symposium (APSURSI)*. 2013, pp. 2119–2120.